1-1-2006

Phenol degradation by combined photochemical-biological wastewater treatment system : kinetic modeling and optimization

Maryam Edalatmanesh
Ryerson University

PHENOL DEGRADATION BY COMBINED PHOTOCHEMICAL-BIOLOGICAL WASTEWATER TREATMENT SYSTEM: KINETIC MODELING AND OPTIMIZATION

by

Maryam Edalatmanesh
(B.Sc., Sharif University of Technology, Iran, 2004)

A thesis
Presented to Ryerson University
In partial fulfillment of the
Requirements for the degree of
Master of Applied Science
in the Program of
Chemical Engineering

Abstract

Phenol Degradation by Combined Photochemical-Biological Wastewater Treatment System: Kinetic Modeling and Optimization

Maryam Edalatmanesh
MASc, Chemical Engineering Program
Ryerson University
Toronto, 2006

A dynamic kinetic model, for the oxidation of phenol in water by UV/ H_2O_2 system is developed. The model is based on elementary chemical and photochemical reactions, initiated by the photolysis of hydrogen peroxide into hydroxyl radical. Numerical values of chemical reaction rate constants and photochemical parameters are taken from literature. The model is validated with data on the oxidation of phenol in the simulated and the actual UV/ H_2O_2 system. Using experimental data from literature, kinetic rate constants for the reactions involving phenol oxidation intermediates, catechol and hydroquinone, are estimated. The rate constants for the reactions, where phenol oxidized to catechol and hydroquinone by hydrogen peroxide are 9×10^8 and 2×10^8 s^{-1} M^{-1}, respectively. The reaction rate constants for oxidations of catechol and hydroquinone by hydrogen peroxide are found to be 9×10^8 and 8×10^7 s^{-1} M^{-1}, respectively.

Phenol biodegradation is best represented by a two-step Haldane model. Both photochemical and biological models are coupled together to give one single chemical-biological system. The photochemical-biological process is optimized for the retention time, electrical energy consumption, and cost. The optimization approach is solved using the Successive Quadratic Programming (SQP) method.

The least retention time for this system is determined to be 99 h and the optimal electrical energy consumption occurs at a photochemical retention time of 15 h and a biological retention time of 92 h.

Calculations on the total cost for different retention times show that the incurred cost by the photochemical unit is considerably higher than that by the biological unit. However, the minimum total cost is evaluated to occur at 15.5 h of photochemical retention time and 90 h of biological retention time.

Acknowledgement

I am greatly indebted to Professor Mehrab Mehrvar and Professor Ramadhane Dhib for their unwavering commitment towards me. Their unique way of addressing the real engineering issues and their practical view is always a model for my academic life. In addition, their financial support to complete this study is highly appreciated.

I sincerely thank my parents for their never-ending support and commitment. I also greatly appreciate the encouragements and patience of my husband, Amir, who also helped me in proofreading my thesis.

Last but not least, the financial support provided by the NSERC is gratefully appreciated. Also the partial financial support from Ryerson University to complete this study is acknowledged.

This thesis is dedicated to my parents whose love, patience, and sacrifice have made me who I am.

Also to my husband for his never ending love, support, and encouragement.

Table of Contents

List of Figures

List of Tables

Nomenclature

A_t	Total absorbance of the solution (Dimensionless)
b	Optical path length (m)
CC	Capital cost ($)
C_C	The concentration of compound C (M)
C_{tot}	Total concentration of HO_2^- and H_2O_2 (M)
c	Velocity of light in vacuum (m s^{-1})
E	Energy (J or kJ)
E_{EM}	Electrical energy required to degrade a unit mass of contaminant (kWh kg^{-3})
E_{EO}	Electrical energy per order of magnitude in a unit volume (kWh m^{-3} per order)
E_λ	Radiation energy of wavelength λ (kJ mol^{-1})
$E_{\lambda D}$	Bond dissociation energy (kJ mol^{-1})
E°	Molar energy (kJ mol^{-1})
e	Blower efficiency (Dimensionless)
f_C	The fraction of UV irradiation absorbed by compound C (Dimensionless)
h	Planck's constant $(6.6256\times10^{-34}\ J.s)$
$k_{2\text{-}19}$	Reaction rate constants of reactions R1-R15 occurring during phenol oxidation in a UV/H_2O_2 system (s^{-1} M^{-1} or s^{-1})
k_a	Equilibrium constant (Dimensionless)
k_i	Inhibition constant (mg L^{-1})
k_s	Half-saturation constant (mg L^{-1})
I_0	Incident UV light intensity (Eins. m^{-3} s^{-1})
M	Molecular weight (g mol^{-1}or kg mol^{-1})
OM	Operating and maintenance cost ($)
P	Power (kW)
$P_{1,2}$	Products of phenol degradation (mg L^{-1})

P_w	Blower power (kW)
P_λ	Spectral radiant power (W)
$p_{1,2}$	Absolute pressure (atm)
Q	Volumetric flow rate (L h^{-1})
Q_i	Volumetric flow rate of the inlet flow (L h^{-1})
Q_W	Volumetric flow rate of the waste sludge (L h^{-1})
Q_r	Volumetric flow rate of the recycled sludge (L h^{-1})
R	Gas constant (kJ $kmol^{-1}$ ^oK)
r_C	Reaction rate of compound C in the system (M s^{-1})
S	Substrate concentration (mg L^{-1})
S_1	Phenol concentration as substrate (mg L^{-1})
S_2	Major metabolic intermediate of phenol degradation (mg L^{-1})
t	Time (s for kinetic rate equations/ h for retention times)
V	Reactor volume (L)
V_B	Bioreactor volume (L)
V_C	Chemical reactor volume (L)
w	Air flow rate (kg s^{-1})
X_1	H_2O_2 concentration in the UV/H_2O_2 system (M)
X_2	H^+ concentration in the UV/H_2O_2 system (M)
X_3	$\dot{O}H$ concentration in the UV/H_2O_2 system (M)
X_4	$HO_2^{\bullet}$ concentration in the UV/H_2O_2 system (M)
X_5	$O_2^{\bullet -}$ concentration in the UV/H_2O_2 system (M)
X_6	Phenol concentration in the UV/H_2O_2 system (M)
Y	Cell yield coefficient (mg biomass/ mg removed substrate)
Z	Biomass concentration (mg L^{-1})
Z_1	Biomass growing on phenol (mg L^{-1})
Z_2	Biomass growing on metabolic intermediate of phenol degradation (mg L^{-1})
α	Recycled sludge to the inlet flow rate ratio (Dimensionless)

ε	Molar extinction coefficient (M^{-1} m^{-1})
γ	Ratio of the waste sludge to the inlet flow rate, Q_W/Q_i (Dimensionless)
ν	Frequency (s^{-1})
$\overline{\nu}$	Wave number (m^{-1})
λ	Wavelength (m or nm)
λ_D	Threshold wavelength (nm)
μ	Specific growth rate (h^{-1})
μ_m	Maximum specific growth rate (h^{-1})
θ_B	Hydraulic retention time in the bioreactor (h)
θ_C	Hydraulic retention time in the chemical reactor (h)
ϕ_C	Quantum yield of compound C

Abbreviations

ACGIH	American Conference of Governmental Industrial Hygienists
CSTR	Continuous Stirred Tank Reactor
CMBR	Completely Mixed Batch Reactor
DBCP	1,2-dibromo-3-chlorophenol
GRG	Generalized Reduced Gradient
IUPAC	International Union of Pure and Applied Chemistry
LD	Lethal Dose
SQP	Sequential Quadratic Programming
TLV	Threshold Limit Value
UV	Ultraviolet
VOC	Volatile Organic Compound
2-hmas	2-Hydroxymuconic acid semialdehyde

CHAPTER 1

INTRODUCTION

Conventionally, attention received by biological oxidation processes surpasses that of the chemical and physical treatment systems, as a result of their cost effectiveness and versatility in handling a wide variety of organic pollutants. However, some organics are either non-biodegradable or toxic to the biological process and must, therefore, be pre-treated. Phenol is one of these biorefractory compounds. Phenolic compounds, especially phenol, are widespread pollutants and are found in many industrial effluents such as wastewater from coal processing plants, resin manufacturing plants, fruit processing industries, oil refineries, and even olive oil mills. The toxicity of phenol to humans and aquatic life imposes its priority of destruction in water. Even small concentrations of phenol or other phenolic compounds can cause antibacterial actions in wastewater. The limiting concentration of phenolic compounds without inhibitory effects has been reported between 400 and 600 ppm (Tuncel and Nergiz, 1993). Moreover, phenolic compounds can slow down or even inhibit the degradation of other contaminants. Therefore if mixed contamination has to be treated, treatment of phenol has the highest priority over the treatment of other contaminants (Stegmann et al., 2001).

Although biological treatment is a well established and cost effective technology, for the degradation of phenol it has been proven to be inefficient due to its biorefractory nature. If the concentration of phenol is beyond 1450 mg/L, the biological reactor would be destabilized, resulting in a discharge of the phenolic pollutants partially treated, i.e. practically untreated (Nuhoglu and Yalchin, 2005).

Available technologies to deal with phenolic compounds include the use of Advanced Oxidation Processes (AOPs). Advanced oxidation is an oxidation process which generates hydroxyl radicals, species of high oxidizing power that react unselectively with the matter present in the water. Chemical oxidation of phenolic wastewaters can be an

alternative treatment scheme when phenol concentration is very high for direct biological systems.

In photolysis, UV light with the wavelength energy of higher than a chemical bond energy can break the chemical bond directly. While in the case of UV/H_2O_2 radiation, UV light with a wavelength lower than 280 nm is able to photolyze hydrogen peroxide molecule and produces two hydroxyl radicals. With regard to the UV processes, the degradation rate with the UV/H_2O_2 process is almost 5 times higher than that of photocatalysis and UV alone (Esplugas et al., 2002). UV/H_2O_2 process potentially allows complete mineralization of organic carbon to carbon dioxide (Bolduc and Anderson, 1997). The main disadvantage of advanced oxidation technologies is that they are expensive compared to the conventional biological systems (Gimeno et al., 2005). Combining chemical and biological processes may result in a more cost effective process with complete degradation of toxic chemicals.

It is important to study the effect of system variables such as phenol concentration, H_2O_2 concentration, flow rates, and reactor characteristics on the system efficiency (Scott and Ollis, 1996). Hence, the combined chemical-biological model can be used for optimizing pollutant removal and minimizing cost. Modeling of the advanced oxidation process is a useful tool for studying the process parameters, and therefore, the system optimization and determination of the best parameters for the process design. Also a kinetic model for the combined process would be required for the design of combined process.

As such, the main objective of this work was to minimize the incurred cost and the retention time, required for efficient phenol removal in a photochemical-biological treatment system. Before attempting any optimization scheme, a good mathematical model describing the degradation process is required. In fact, a dynamic mathematical model based on the chemical and photochemical principles for phenol degradation in a UV/H_2O_2 system was developed. It was validated using data collected from literature. Furthermore, to establish an overall photochemical-biological model for the combined process, this photochemical model was combined with an existing biological model for

the biodegradation of phenol found in the literature. Few optimization schemes are proposed to determine the best operating conditions of the combined process so that the phenol removal is maximized at the lowest overall cost.

The remainder of this thesis is organized as follows. Chapter 2 provides an overview of the phenol contamination, the advanced oxidation process, and the related results available in the literature. A kinetic model for the UV/H_2O_2 system is developed and validated in Chapter 3, while the details of the applied biological model are provided in Chapter 4. Chapter 5 includes the simulation and optimization results using the overall model. Finally, some concluding remarks and recommendations for further research are provided in Chapter 6.

CHAPTER 2
LITERATURE BACKGROUND

2.1 Phenol

Phenol is an aromatic molecule with hydroxyl group attached to the benzene ring structure, as depicted in Figure 2.1.

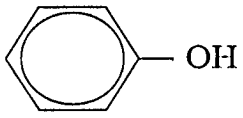

Figure 2.1: Molecular structure of phenol

It is a colorless to pink, hygroscopic solid with a comfortable odor characteristic that can be detected in air at 0.04 ppm (ACGIH, 2001). Chemical and physical properties of pure phenol are presented in Table 2.1.

Table 2.1: Chemical and physical properties of pure phenol (ACGIH, 2001)

Chemical/Physical Property	Value
Molecular weight	94.11 g/mol
Specific gravity	1.071
Melting point	43°C
Boiling point	182°C
Vapor pressure	0.35 torr at 25°C
Concentration in saturated air	0.046% volume at 25°C
Flash point, closed cup	79°C
Flash point, open cup	85°C
Explosive limits	1.7-8.6%
pK_a	10.0 at 25 atm
pH (aqueous solution)	6
Solubility in water	6.67×10^{4} mg/L

2.1.1 Sources of Phenol Pollution

Phenol is a widespread pollutant found in many industrial effluents such as wastewater from coal processing plants, oil refineries, pulp and paper manufacturing plants, resins and coke manufacturing, steel industries, pharmaceutical industries, paint, textile, pesticide plants, tannery, etc. Phenol serves as intermediate in the industrial synthesis of products as diverse as adhesives and antiseptics (Alnaizy and Akgerman, 2000). Catechol and chlorophenol existing in many industrial wastewaters are two major pollutants from the phenol group.

2.1.2 Health Hazards Caused by Phenol

Due to their inherent toxicity, phenolic compounds are prone to accumulate in water and soil after being discharged if no adequate treatment has been done. Phenols are toxic to human, fish and to several biochemical functions. U.S. Department of Health and Human Services has reported phenol to be very toxic to humans through oral exposure, with ingestion of 1 g to be lethal, with symptoms including muscle weakness and tremors, loss of coordination, paralysis, convulsions, coma, and respiratory arrest. Blood changes, liver and kidney damage, and cardiac toxicity including weak pulse, cardiac depression, and reduced blood pressure have been reported in humans acutely exposed to phenol by the oral route (Nuhoglu and Yalchin, 2005). Due to these adverse health effects of phenols, the World Health Organization (WHO) has set a limit level of 1 $\mu g\ L^{-1}$ to regulate the phenol concentration in drinking waters.

Acute toxicity is a property of a substance that has toxic effects on living organisms, when that organism is exposed to a lethal dose of the substance once. The LD_{50} or semi-lethal dose of a particular substance is a measure of how much constitutes a lethal dose. The acute oral LD_{50} of phenol in rats, dogs, rabbits, and monkeys is reported to be about 530 mg per kg of body mass (ACGIH, 2001). In human cases, studies show that death is a common outcome of the acute phenol poisoning which occurs mostly as a result of skin absorption. The Threshold Limit Value - Time Weighted Average (TLV-TWA) of a chemical substance defines the reasonable level to which a worker can be exposed during

average exposure on the basis of an 8 h/day, 40 h/week work schedule without adverse effects. A TLV-TWA of 5 mg/L is recommended for phenol.

2.1.3 Treatment of Phenol

Phenol biodegradation by microbial biomass is known to be inhibited by phenol itself. Even small concentrations of phenol or other phenolic compounds can inhibit the microbial growth. Moreover, wastewater containing phenol may be difficult to treat since phenolic compounds can slow down or even inhibit the degradation of other contaminants (Stegmann et al., 2001). The ability to degrade phenol and other phenolic compounds is widespread in mesophilic microorganisms. *Pseudomonas* species have been used in phenol degradation studies and were shown to be capable of degrading phenol (Stegmann and Brunner, 2001). The limiting concentration of phenolic compounds without inhibitory effects is observed in the range of 270 to 1750 mg/L for different microbial species (Neumegen et al., 2005; Arutchelvan et al., 2006). The limiting concentration considered in this study is 1450 mg/L as reported for activated sludge by Nuhoglu and Yalchin (2005). Biological processes fail to treat wastewater with phenol concentration exceeding this limit. Alternatively, chemical oxidation is deemed a promising treatment.

Available technologies to treat phenolic compounds include the use of advanced oxidation processes, AOPs (Gimeni et al., 2005). The main drawback of these technologies is economical. For this reason, combined chemical-biological processes are suggested to treat phenol more efficiently and economically.

2.2 Advanced Oxidation Processes (AOPs)

An AOP is an oxidation process generating hydroxyl radicals in sufficient quantity to affect water treatment (Glaze, 1987). Usually, a combination of oxidation agents (such as H_2O_2 or O_3), irradiation (such as UV or ultrasound), and catalysts (such as metal ions or semiconductors) are employed to generate hydroxyl radicals. . Table 2.2 lists different chemical processes suitable for water and wastewater treatment.

Table 2.2: Examples of AOPs evaluated for water and wastewater treatment (Parsons, 2004)

Catalysis	Pulsed plasma
Fenton's reagent	Ultrasound
Ferrate	UV
Electrochemical	UV/H_2O_2
Wet air oxidation	$UV/H_2O_2/O_3$
Photo-Fenton's reagent	Vacuum UV
Photocatalysis	UV/O_3

A few of them have been explained as follows:

Fenton/ photo-Fenton process

Fenton process is being used in treating contaminated water or soil. This process involves the use of one or more oxidizing agents such as hydrogen peroxide or oxygen, and a catalyst which is usually iron salt or oxide. Photo-Fenton or photo-assisted Fenton also involves irradiation which raises the rate of contamination degradation. The Fenton reagents, mainly hydrogen peroxide and iron salts, are not expensive and non-toxic. The Fenton process is only efficient in the pH range 2-4 (Parsons, 2004).

Semiconductor photocatalysis process

In semiconductor photocatalysis process, a semiconductor material such as TiO_2 is the light absorbing species. This semiconductor usually acts as a photosensitizer, since it is able to support thermodynamically feasible reactions without being changed itself. The overall process can be represented as follows (Parsons, 2004):

$$\text{Pollutant} + O_2 \xrightarrow{Semiconductor,h\nu} \text{minerals} \qquad (2.1)$$

Ultrasound process

The ultrasound treatment is the results of ultrasonically induced acoustic cavitation. It causes chemical and physical changes in a liquid medium through the generation and

subsequent destruction of cavitation bubbles. The sound ranges employed are those that can generate cavitation. Large-scale applications are mainly in the 20-40kHz range.

Wet air oxidation processes

Wet oxidation is the process of oxidizing suspended or dissolved pollutants in water with dissolved oxygen at high temperature. It is known to be efficient for treatment of waste streams which are too dilute to be incinerated. It requires much less energy compared to incineration.

Pulsed plasma process

In a pulse-plasma incinerator, a high-energy, high-density pulsed-plasma jet goes through the fluid material bed that has to be treated. Because of the large interface area between the jet and the fluid, the efficiency of the radiative heat transfer is higher, by several order of magnitude, than the UV irradiation. It is usually being used for the degradation of complex organic dyes (Sugiarto et al., 2002)

The oxidation potential of an oxidant is related to its oxidation-reduction potential (E°). An oxidant with a high E° value is a strong oxidation agent. Many oxidants are 'free radicals', of which the hydroxyl radical, $\dot{O}H$, is the most powerful oxidizing species after fluorine (see Table 2.3).

Table 2.3: Oxidation potential of common species (Parsons, 2004)

Species	Oxidation potential (V)
Fluorine	3.03
Hydroxyl radical	2.8
Atomic oxygen	2.42
Ozone	2.07
Hydrogen peroxide	1.78
Perhydroxyl radical	1.7
Permanganate	1.68
Hypobromous acid	1.59
Chlorine dioxide	1.57
Hypochlorous acid	1.49
Chlorine	1.36

A free radical is not an ionic species but it is formed from an equal cleavage of a double electron bond. Free radicals may be generated using UV radiation by the homogenous photochemical degradation of oxidizing compounds such as hydrogen peroxide or ozone. One way of generating hydroxyl radicals is through the cleavage of H_2O_2 in the presence of UV with a wavelength of less than 280 nm:

$$H_2O_2 \longrightarrow 2^{\bullet}OH \qquad (2.2)$$

Hydroxyl radical ($\dot{O}H$) is a powerful and non-selective chemical oxidant, which reacts rapidly with most organic compounds. Comparing the reaction rate constants of ozone to hydroxyl radical, when reacting with some organic compounds, Table 2.4, shows that the hydroxyl radical is able to oxidize organic compounds about 10^8 times faster than ozone. Yet, ozone is considered to be a powerful oxidant.

Table 2.4: Comparison between rate constants of ozone and hydroxyl radicals for a range of compounds.

Organic compound	Rate Constant ($s^{-1} M^{-1}$)	
	O_3	$^{\bullet}OH$
Chlorinated Alkenes	10^{-1}-10^{3}	10^{9}-10^{11}
Phenols	10^{3}	10^{9}-10^{10}
N-containing organics	10-10^{2}	10^{8}-10^{10}
Aromatics	1-10^{2}	10^{8}-10^{10}
Ketons	1	10^{9}-10^{10}
Alcohols	10^{-2}-1	10^{8}-10^{9}
Alkanes	10^{-2}	10^{6}-10^{9}

Based on the organic species, different reactions may happen:

- Addition of a hydroxyl radical to the contaminant
- Abstraction of a hydrogen atom
- Electron transfer to a halogenated compound

2.2.1 UV Light-Based Applications

Photo-activated chemical reactions are characterized by free radical mechanism initiated by the interaction of photons of a proper energy level with molecules of the chemical species present in the solution, with or without the presence of a catalyst (Gogate and Aniruddha, 2003). Photochemical technologies are clean, efficient, and usually beneficial to both environmental contaminant treatment and wastewater disinfection. On the other hand, employing the UV systems entails considerable disadvantages such as high cost of equipment, operation and maintenance, which depends on several factors, such as water quality, system design, UV lamps cost, electrical energy cost, as well as the oxidant dosage (Parsons, 2004).

The contaminant absorbs the incident UV radiation and undergoes degradation starting from its excited state. The fact that the light absorption by the target pollutant is essential

in the UV photolysis process, limits the industrial applications of the UV systems compared to the hydroxyl radical driven technologies.

The UV/H_2O_2 process is based on the generation of powerful oxidizing, hydroxyl radical, through the direct photolysis of hydrogen peroxide. In this method, the UV absorption by the target pollutant is not absolutely required which makes this technology more reliable.

UV/ H_2O_2 process has several applications in water and wastewater treatment as follows (Parsons, 2004):

- Removal of pollutants from drinking water;
- Removal of the disinfection by-products and their precursors from drinking water;
- Treatment of toxic organics in groundwater;
- Treatment of contaminated soil washing water;
- Control of off-gas emissions from volatile organic compound (VOC) stripping.

2.2.2 Photolysis

Light is an electromagnetic radiation and has both wave and particle properties. The relationship between the wavelength λ (m or nm) and the frequency ν (s^{-1}) of radiation is defined by:

$$\lambda = \frac{c}{\nu} \tag{2.3}$$

where $c = 3.0 \times 10^8 m.s^{-1}$ is the speed of light.

Light is absorbed or emitted in discrete units of energy E, called quanta or photons ($h\nu$), which are related to the frequency of radiation through this equation:

$$E = h\nu = \frac{hc}{\lambda} = hc\bar{\nu} \tag{2.4}$$

where $h = 6.6256 \times 10^{-34} J.s$ is Planck constant, and $\bar{\nu}$ is the wave number (m^{-1}).

UV radiation is defined as the electromagnetic radiation of wavelength between 4 and 400 nm. In other words, it is the spectral domain that covers the gap between the X-ray and the visible region. The UV spectral range of interest in wastewater treatment is 200-280 nm, where the pollutants absorb the radiation (Parsons, 2004). Observing the energies carried by UV radiations with different wavelengths, they can be compared with energies required for chemical bond dissociation (Table 2.5).

In Table 2.5, ΔE° (kJ.mol^{-1}) is the single bond dissociation energy and λ_D (nm) is the corresponding 'threshold' wavelength, defined as the maximum wavelength for which the photon energy matches the bond energy required to result in a homolytic bond cleavage.

Table 2.5: Bond dissociation energies and corresponding light 'threshold' wavelengths (Parsons, 2004 and references therein)

Bond	$\Delta E^{\circ}(kJ/mol)$	$\lambda_D(nm)$
C_6H_5—H	428	279
n-C_3H_7—H	407	294
C_6H_5—OH	371	322
H_3C—CH_3	349	343
H_3C—Cl	340	352
C_2H_5O—NO	244	490
H_2N—NH_2	236	507
HO—HO	211	568

Theoretically, any radiation of $\lambda < \lambda_D$, carrying an energy $E_\lambda > E_{\lambda D}$, can break the corresponding chemical bond, as a result of light absorption. However, that process taking place is determined by two factors:

1. The probability of the light absorption event, which relates to the properties of the compound that are quantified in its absorption spectrum.
2. The possibility that the reached excited state proceeds to a chemical reaction, which is expressed as the quantum yield.

The absorption spectrum characteristics depend on the molecular structure of the absorber and its interactions with the solvent. Most UV absorbers contain double bonds or conjugated double bonds involving carbon, nitrogen or oxygen atoms. These chemical groups, capable of selective light absorption, are called "chromophores". They are usually characterized by delocalized $\pi-$electrons. Saturated compounds containing the same atoms do not absorb light with a wavelength of more than 205-210 nm, and therefore, cannot be treated economically by a direct UV photolysis technology.

The reaction quantum yield is one of the most important parameters in evaluating the efficiency of a photochemical process. It covers all reactions in a given set of conditions that lead to the decay of the parent pollutant X_i as a result of light absorbed. Based on the first law of photochemistry (Grotthus-Draper law), only the light that is absorbed by a molecule can be effective in producing photochemical changes in that particular molecule. The International Union of Pure and Applied Chemistry (IUPAC) has defined the quantum yield for photochemical reactions as the amount of reactant consumed per amount of photons absorbed. Therefore, the quantum yield for direct UV photolysis of X_i is defined as:

$$\phi_r(\lambda) = \frac{\text{total number of moles of } X_i \text{ transformed}}{\text{total number of moles of photons of } \lambda \text{ absorbed by } X_i \text{ in the system}} \qquad (2.5)$$

$\phi_r(\lambda)$ is defined for the monochromatic radiation. Its numerical value for each absorbing compound depends on the irradiation wavelength. It can also be defined in terms of kinetics (Parsons, 2004):

$$\phi_r(\lambda) = \frac{-\frac{d[X_i]}{dt}}{I_{a,X_i}(\lambda)} \tag{2.6}$$

where $I_{a,C_i}(\lambda)$ is the intensity for the light absorbed by X_i. Light intensity can also be expressed with Ein s^{-1}, where Ein is defined as one mole of photons per liter.

When light with an initial intensity I_o at a specified wavelength λ passes through a solution, photons are partly absorbed by the light-absorbing species in the solution and thus, light would leave the solution with a lower intensity I.

The absorbance A is the measure of the amount of radiant power absorbed by a sample and it is defined by the following equation (Oppenlander, 2003):

$$A_\lambda = -\log(I/I_o) \tag{2.7}$$

Beer-Lambert law or Beer-Lambert-Bouguer law states that the fraction of light absorbed by a system does not depend on the incident spectral radiant power, and the absorbance is proportional to the number of the constituent molecules absorbing the radiation. It can be concluded that there is a linear relationship between the absorbance and the concentration of the absorbing species. Hence, Beer-Lambert law can be expressed as:

$$A_\lambda = \varepsilon.b.X_i \tag{2.8}$$

where ε is the wavelength-dependent molar absorptivity coefficient (cm^{-1} M^{-1}), b is the

path length (cm), and X_i is the concentration of the pollutant (M). M is the molarity of the compound in solution.

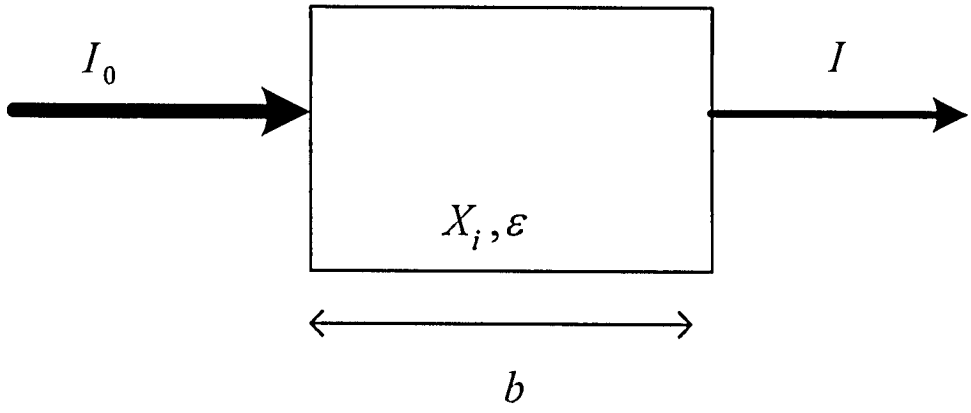

Figure 2.2: Light intensity propagation through a solution with concentration X_i

Under monochromatic radiation λ, the rate of direct photolysis of a pollutant X_i may be expressed by rewriting equation (2.6) as follows:

$$-\left(\frac{d[X_i]}{dt}\right)_\lambda = \phi_r(\lambda) I_{a,X_i}(\lambda) \tag{2.9}$$

From Figure 2.2, the light intensity absorbed by all components in the solution is:

$$I_a = I_o - I \tag{2.10}$$

The ratio of the light absorbed by component X_i to that absorbed by all components in the solution is denoted by f_i (X_i is the i^{th} compound). Therefore, the light intensity absorbed by X_i is simply:

$$I_{a,X_i} = f_i I_a \tag{2.11}$$

where f_i is expressed by the following equation (Oppenlander, 2003):

$$f_i = \frac{\varepsilon_i X_i}{\sum_j \varepsilon_j X_j} \tag{2.12}$$

f_i is the fraction of UV irradiation absorbed by the light-absorbing species *i*. It is the ratio of the light absorbed by the species *i* to the total light absorbed by the solution. ε_i is the molar absorptivity (extinction) coefficient of the i^{th} species at the lamp wavelength. Further, the extinction coefficient ε_i is the summation of the absorption coefficient and the scattering coefficient. It depends on the wavelength, the particle shape, the size distribution of the particles, and the refractive index of the particles, which is related to the chemical composition.

The total absorbance I_a of the solution, based on equations (2.7) and (2.10), it should be expressed as follows:

$$I_a = I_o(1-10^{-A_t}) \tag{2.13}$$

where A_t is the total absorbance of the solution which can be calculated through the following equation:

$$A_t = b\sum \varepsilon_i [X_i] \tag{2.14}$$

where b is the (effective) pathlength of the photoreactor.

The photolysis rate defined in equation (2.9) becomes:

$$r_{UV,i} = -\frac{dX_i}{dt} = \phi_i f_i I_o\left(1-10^{-A_t}\right) \tag{2.15}$$

where b is the reactor pathlength (m); ϕ_i and ε_i are the quantum yield and the extinction coefficient of the degrading compound, respectively.

2.2.3 Efficiency of AOPs

The evaluation of efficiency of advanced oxidation technologies, with respect to the electrical energy consumption related to the contaminant removal, is defined in the literature (Bolton et al., 1995).

The electrical energy E_{EM} required to degrade a unit mass of a contaminant X in polluted water or air is expressed as:

$$E_{EM} = \frac{Pt}{VM(X_i - X_f)} \tag{2.16}$$

where P is the power of the UV source, V is the volume of the wastewater treated during time t (h), M is the molecular weight of the contaminant X, X_i and X_f are the initial and final concentrations of the contaminant, respectively.

Also, the electrical energy E_{EO} required to degrade a contaminant X by one order of magnitude in a unit volume is expresses for two regimes of operation as follows:

Batch operation:
$$E_{EO} = \frac{Pt1000}{V\log(X_i/X_f)} \tag{2.17}$$

Continuous operation:
$$E_{EO} = \frac{P}{Q\log(X_i/X_f)} \tag{2.18}$$

where Q is the water flow rate and 1000 is the conversion factor (l /m^3). E_{EO} combines light intensity, residence time and percent destruction into a single quantity. The total

energy requirement depends on the initial concentration of the contaminant and the required purification efficiency.

2.3 Mathematical Modeling of a Dynamic System

A mathematical model is an abstract representation used to describe the behavior of a system. It allows analyzing physical and biological systems. Dynamic modeling leads to the development of differential equations for which analytical solutions are not always obvious. Alternatively, numerical solutions are sought. Numerical modeling is a superset of mathematical modeling. Numerical modeling contains the original mathematical modeling descriptions, but creates approximations to mathematical model solutions. Numerical modeling essentially converts an analytical solution into an approximate algebraic solution to determine the unknown coefficients.

2.4 Previous works on the modeling of AOPs

The practical application of UV/ H_2O_2 process requires the determination of the design and operational variables. Table 2.6 summarizes works in the open literature done on kinetic modeling and/or experimental studies of photolytic and non-photolytic systems. Most of the organic compounds studied were degraded by direct UV irradiation. It has been observed that the use of H_2O_2 accelerates the decomposition of organics except for few pesticides. Generally, the degradation of organic compounds has been modeled as single component systems where only the disappearance of the model compound is followed. In most cases, the by-products formed during the degradation process were neglected.

Laboratory scale experiments with synthetic single-compound solutions are numerous, but only two modeling approaches based on chemical and photochemical principles have been developed by Glaze et al.(1995) and Crittenden et al. (1999) who used 1,2-dibromo-3-chlorophenol (DBCP) as the model compound. The models were used to predict the DBCP concentration as a function of time for different concentrations of hydrogen peroxide. The models were verified against experimental data.

Glaze et al. (1995) used the pseudo-steady state approximation to describe the kinetics of free radical species in the UV system.

Crittenden et al. (1999) did not employ the pseudo-steady state assumption rendering their model much more reliable.

The kinetic models proposed by Gallard and De Laat (1999) and Kang et al. (2002) for Fenton system are also worth mentioning for their inclusive suggested reaction mechanism, even though there was no photolytic reaction in their system.

Gallard and De Laat (1999) utilized atrazine as the model compound. Their model consists of 8 differential equations; however, they did not consider propagation and termination reactions. Their model is in good agreement with experimental data.

Kang et al. (2002) used phenol and chlorophenols as model compounds. They proposed a comprehensive reaction mechanism.

The remaining references in Table 2.6 are experimental works on synthetic solutions. In some cases, rate expressions also have been developed. It should be noted, however, such expressions are basically interpolations of the experimental data where authors ignored all of the underlying complex chemical and photochemical reactions. Moreover, the rate constants obtained via such methods are specific to the particular experimental setup and should be re-evaluated with any change in the setting or initial concentrations. Table 2.6 also shows the reactions in common with the reaction mechanism proposed in this work, Section 3.1.

Table 2.6: Modeling of different AOPs

Chemical Treatment	Substrate (Model compound)	Kinetic Model	Experimental Process	Reactions in common	Reference
UV/H_2O_2	Phenol	A simplistic kinetic model with pseudo-steady state assumption, Constant pH assumption.	Completely batch photolytic reactor	R1, R2, R4,R9,R10	Alnaizy and Akgerman (2000)
UV/H_2O_2	DBCP	A reliable kinetic model, Carbonate and bicarbonate scavenging effect is taken into account, no pH effect is considered.	Batch photolytic reactor	R1,R2,R3,R4, R5,R8,R9, R10,R11,R12	Glaze et al. (1995)
UV/H_2O_2	4-Nitrophenol	A pseudo-first order rate expression, No reaction mechanism, based on experimental data.	Batch photolytic reactor	No reaction mechanism	Zhang et al., (2003)
UV/H_2O_2	Malachite Green (MG)	A pseudo-first order rate expression, No reaction mechanism, based on experimental data.	Batch photolytic reactor	No reaction mechanism	Modirshahla and Behnejadi (2005)
Fe^{2+}/H_2O_2	Phenol and monochlorphenols	Kinetic model for non-photolytic system	Batch and semibatch non-photolytic	R2,R6,R7,R8, R9,R10,R11, R12,R14	Kang et al., (2002)

Chemical Treatment	Substrate (Model compound)	Kinetic Work	Experiment	Reactions in common	Reference
Fe^{2+}/H_2O_2	Atrazine	Propagation and termination reactions involving organic radicals assumed negligible	Batch non-photolytic reactor	Not comparable	Gallard and De Laat, (1999)
UV/H_2O_2	C. I. Acid Black	A pseudo-first order rate expression, No reaction mechanism, based on experimental data.	Batch photolytic reactor	No reaction mechanism	Shu and Chang, (2005)
UV/H_2O_2	Reactive Black 5	Rate expressions based on experimental data and also few reactions.	Two-part batch reactor	R1,R2,R4,R5	Mohey El-Dein et al., (2003)
UV, O_3, UV/H_2O_2, O_3/H_2O_2, O_3/UV	Phenanthrene and Nitrobenzene	A pseudo-first order rate expression	Semibatch photolytic/non-photolytic	R1,R2,R3,R5 R9,R10,R11, R12	Beltran et al., (1999)
UV/H_2O_2	DBCP	A dynamic kinetic model in a CMBR considering the radical scavengers and pH effect.	Used Glaze et al.(1995) results	R1,R2,R3,R4, R5,R8,R9, R10,R11,R12	Crittenden et al., (1998)

2.5 Previous Works on the Optimization of Biological Treatment Processes

Dynamic optimizations of biological wastewater treatment systems based on mathematical models are scarce in literature.

Rigopoulos and Linke (2002) applied stochastic optimization-based synthesis technology for reaction/separation networks to the activated sludge process design problem. They minimized the COD and the total nitrogen content in the effluent. Due to the stochastic nature of their optimization, different results for different initial designs were obtained.

A dynamic optimization of a small size single basin wastewater treatment plant was presented by Fikar et al. (2001). The objective was to determine an optimal sequence of aeration/non-aeration times subject to the minimization of energy consumption from a control point of view. They used Activated Sludge Model No.1 as their model.

2.6 Concluding Remarks

This chapter provided an overview of the phenol contamination and hazards, the advanced oxidation process, and photolysis theory. Also the related works available in the literature were reviewed in this chapter. In the next chapter a kinetic model for the UV/H_2O_2 system is developed and validated.

CHAPTER 3

KINETIC MODELING OF THE UV/H_2O_2 SYSTEM FOR PHENOL DEGRADATION

3.1 Reaction Mechanism

The mechanism of phenol photochemical oxidation in a UV/H_2O_2 system has been studied extensively. The process mainly depends on the photolysis of H_2O_2 which generates very powerful oxidizing species i.e. hydroxyl radicals. As stated later, the degradation of phenol occurs via two major pathways: direct photolysis by UV irradiation and indirect decomposition with hydroxyl radicals.

3.1.1 Elementary Reactions of H_2O_2 Photolysis

Radiation with a wavelength less than 280 nm is able to decompose H_2O_2 molecule. The mechanism of the hydrogen peroxide photolysis is a cleavage of the H_2O_2 molecule into two hydroxyl radicals with a quantum yield of two hydroxyl radicals per quantum of radiation absorbed as follows:

Initiation:

$$H_2O_2 \xrightarrow{h\nu, k_1} 2^{\bullet}OH \qquad \text{(R1)}$$

Investigations on hydrogen peroxide photolysis have indicated that a number of radical chain reactions take place in a hydrogen peroxide solution with UV-light irradiation as follows:

Propagation:

$$^{\bullet}OH + H_2O_2 \xrightarrow{k_2} HO_2^{\bullet} + H_2O \qquad \text{(R2)}$$

$$^{\bullet}OH + HO_2^{-} \xrightarrow{k_3} HO_2^{\bullet} + OH^{-} \qquad \text{(R3)}$$

$$H_2O_2 + HO_2^{\bullet} \xrightarrow{k_4} {}^{\bullet}OH + H_2O + O_2 \qquad \text{(R4)}$$

$$H_2O_2 + O_2^{\bullet -} \xrightarrow{k_5} {}^{\bullet}OH + O_2 + OH^{-} \qquad \text{(R5)}$$

$$O_2^{\bullet -} + H^+ \xrightarrow{k_6} HO_2^{\bullet} \quad \text{(R6)}$$

$$HO_2^{\bullet} \xrightarrow{k_7} O_2^{\bullet -} + H^+ \quad \text{(R7)}$$

Termination:

$$^{\bullet}OH + ^{\bullet}OH \xrightarrow{k_8} H_2O_2 \quad \text{(R8)}$$

$$^{\bullet}OH + HO_2^{\bullet} \xrightarrow{k_9} O_2 + H_2O \quad \text{(R9)}$$

$$HO_2^{\bullet} + HO_2^{\bullet} \xrightarrow{k_{10}} H_2O_2 + O_2 \quad \text{(R10)}$$

$$HO_2^{\bullet} + O_2^{\bullet -} \xrightarrow{k_{11}} HO_2^{-} + O_2 \quad \text{(R11)}$$

$$^{\bullet}OH + O_2^{\bullet -} \xrightarrow{k_{12}} O_2 + OH^- \quad \text{(R12)}$$

In a UV/H_2O_2 process, hydroxyl radicals produced react rapidly with the organic compounds in the solution, in this case phenol.

3.1.2 Reactions of Phenol

Phenol rapidly reacts with hydroxyl radicals. It can also be degraded directly via UV irradiation:

$$^{\bullet}OH + C_6H_5OH \xrightarrow{k_{13}} \text{intremediates} \longrightarrow CO_2 + H_2O \quad \text{(R13)}$$

$$C_6H_5OH \xrightarrow{h\nu, k_{20}} \text{intermediates} \longrightarrow CO_2 + H_2O \quad \text{(R14)}$$

The most commonly accepted reaction pathway presented for phenol oxidation so far is shown in Figure 3.1 (Devlin and Harris, 1984).

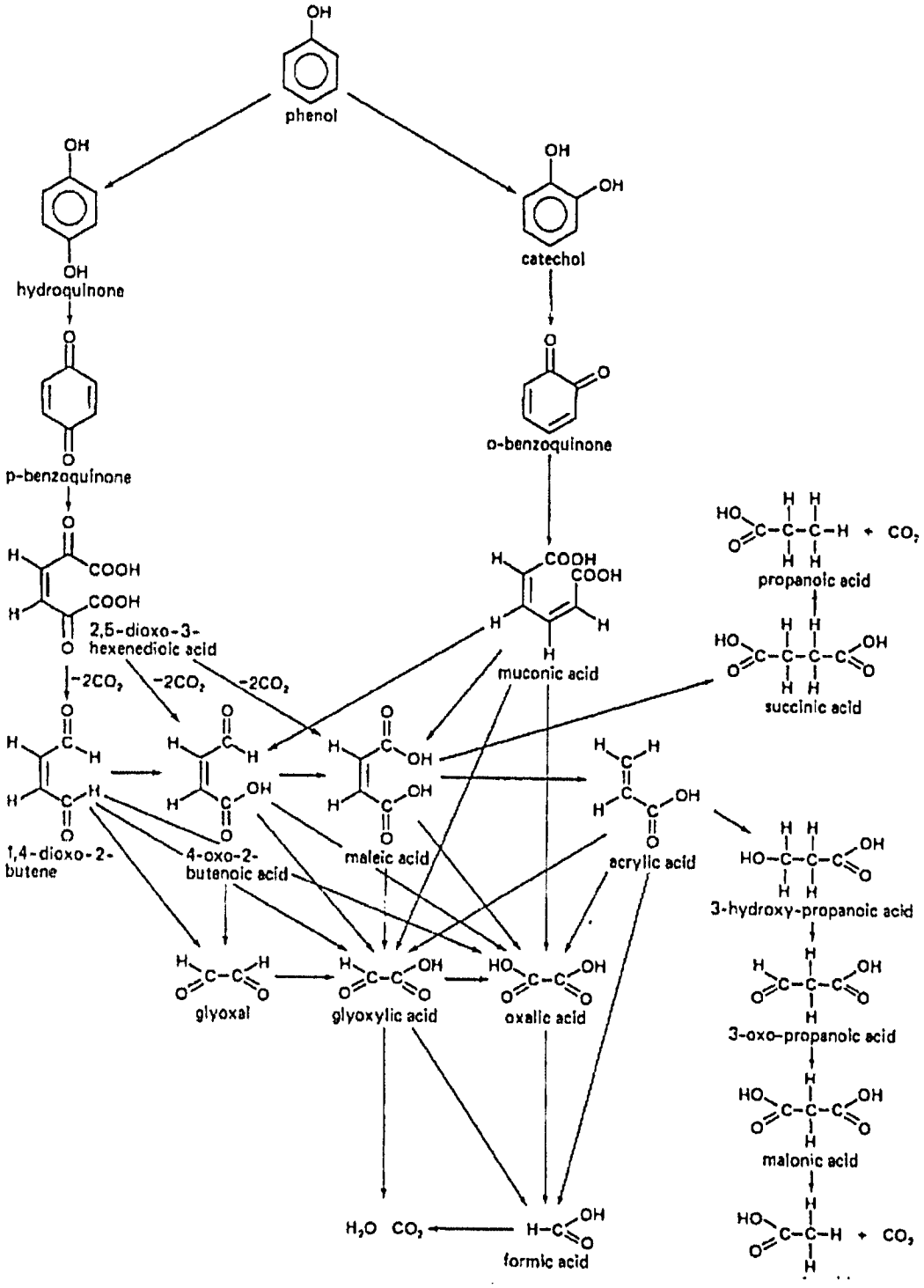

Figure 3.1: Proposed reaction pathway for phenol oxidation by molecular oxygen (Devlin and Harris, 1984)

The oxidation of aqueous phenol by oxygen at elevated temperature and pressure has been studied. Even though, the system used was quite different from UV/H_2O_2 system, their approach to model the pathway of phenol oxidation may be applied in UV/H_2O_2 system as well.

The intermediates of phenol oxidation by UV/H_2O_2 system proposed in the literature (Scheck and Frimmel, 1995; Alnaizy and Akgerman, 2000) are as follows:

$$\text{phenol} + {}^{\bullet}OH \begin{cases} \xrightarrow{k_{14}} 1,2-\text{dihydroxybenzene} \xrightarrow{{}^{\bullet}OH,k_{17}} \text{Organic Acids}/CO_2, H_2O_2 \\ \xrightarrow{k_{15}} 1,4-\text{dihydroxybenzene} \xrightarrow{{}^{\bullet}OH,k_{18}} \text{Organic Acids}/CO_2, H_2O_2 \\ \xrightarrow{k_{16}} 1,3-\text{dihydroxybenzene} \xrightarrow{{}^{\bullet}OH,k_{19}} \text{Organic Acids}/CO_2, H_2O_2 \end{cases} \quad \text{(R15)}$$

The commercial names for 1,2- , 1,3- ,and 1,4- dihydroxybenzene are "Catechol", "Resorcinol" and "Hydroquinone", respectively. Phenol is hydroxylated in the UV/H_2O_2 system to mainly 1,2- and 1,4- dihydroxybenzene and barely to 1,3- dihydroxybenzene, (Devlin and Harris, 1984; Scheck and Frimmel, 1995; Alnaizy and Akgerman, 2000). Dihydroxybenzenes is further oxidized to organic acids which are not harmful to nature. Organic acids can also be oxidized to CO_2 and water by hydroxyl radicals, but their rates are about 10 to 10^2 times lower than the reaction rates of dihydroxybenzenes with hydroxyl radicals (Alnaizy and Akgerman, 2000). Two possible mechanisms for explaining the hydroxylation of phenol have been reported in literature (Scheck and Frimmel, 1995):

1. The hydroxyl radical attacks the phenolic ring and forms an intermediate (cyclohexadienyl radical) which is converted to dihydroxybenzene by hydrogen abstraction.
2. The hydroxyl radical converts phenol to a phenoxyl radical (intermediate) by hydrogen abstraction. Then, the hydroxyl radical is added to the intermediates and results in dihydroxybenzene.

Unfortunately, numerical values for the kinetic rates k_{14} – k_{19} are not reported in literature. The existing kinetic studies (Scheck and Frimmel, 1995; Alnaizy and Akgerman, 2000) have proposed pseudo-first-order kinetic rates for the reactions. Alnaizy and Akgerman (2000) established an exponential relationship between the initial phenol concentration and the k value in their system (Figure 3.2).

Since the experimental results were in straight lines for the semi-logarithmic graphs of the concentration of phenol and the organic acid, it was suggested that the reactions of pseudo-first-order for phenol and its by-products are first order:

$$-\frac{dC}{dt} = kC \tag{3.1}$$

Where C is the concentration of phenol or of an intermediate and k (s^{-1}) is the reaction rate constant of the substrate. Variations in the hydroxyl radical concentration are not considered, rendering the kinetic rates limited for their system specifications. The values reported for k are basically estimated from the experimental data and different values of k are reported in the literature. Thus, even a slight change in the initial concentration of the substrate or hydrogen peroxide concentration calls for a new experiment to evaluate k again. Moreover, phenol reaction rate constants reported by Scheck and Frimmel (1995) and those by Alnaizy and Akgerman (2000) differ by 7 orders of magnitude. Based on the experimental data presented by Alnaizy and Akgerman (2000), the reaction rate constants, k_{14}, k_{15}, k_{17}, and k_{18}, have been determined in Section 3.2.2.

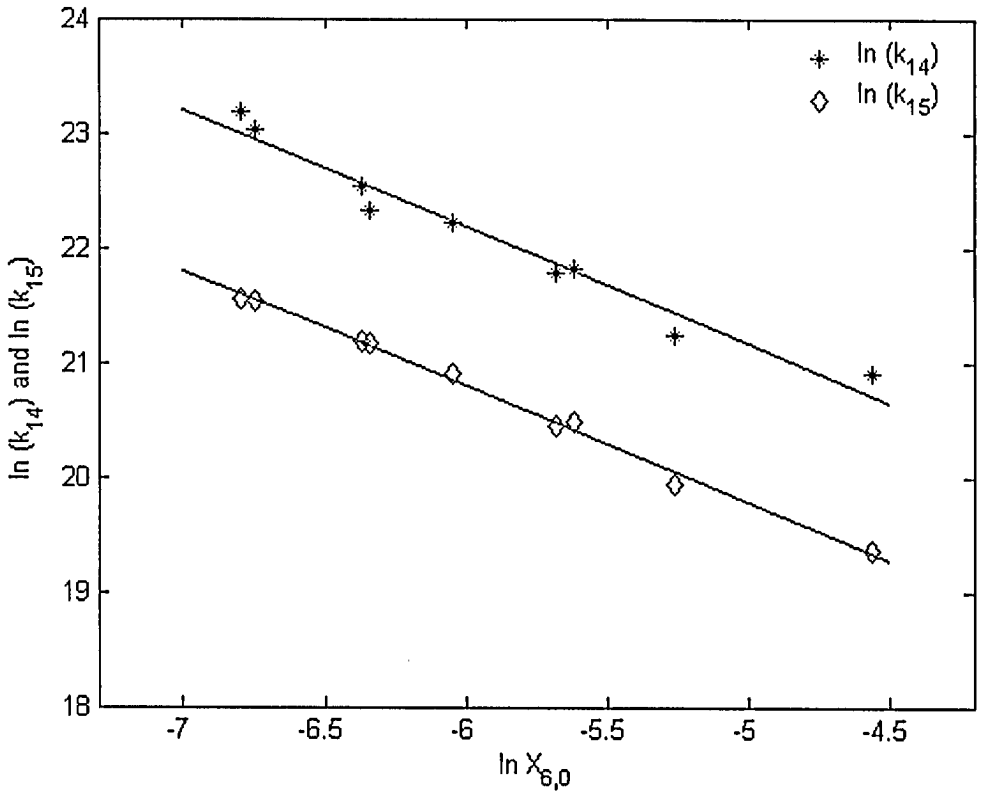

Figure 3.2: Reaction rate constants of catechol and hydroquinone oxidation by hydroxyl radical, as functions of phenol initial concentration (Alnaizy and Akgerman, 2000)

Table 3.1 shows rate constants for the chemical and photochemical reactions occurring in a UV/H_2O_2 system.

Table 3.1: Numerical values of the kinetic rate constants

k	References
$k_2 = 2.7\times10^7 M^{-1}s^{-1}$	(Christensen et al. 1982)
$k_3 = 7.5\times10^9 M^{-1}s^{-1}$	(Christensen et al. 1982)
$k_4 = 3.0 M^{-1}s^{-1}$	(Koppenol et al., 1978)
$k_5 = 0.13 M^{-1}s^{-1}$	(Weinslein et al., 1979)
$k_6 = 1.0\times10^{10} M^{-1}s^{-1}$	(Bielsky et al., 1985)
$k_7 = 1.58\times10^5 s^{-1}$	(Bielsky et al., 1985)
$k_8 = 5.5\times10^9 M^{-1}s^{-1}$	(Buxton et al., 1988)
$k_9 = 6.6\times10^9 M^{-1}s^{-1}$	(Schested et al., 1968)
$k_{10} = 8.3\times10^5 M^{-1}s^{-1}$	(Bielsky et al., 1985)
$k_{11} = 9.7\times10^7 M^{-1}s^{-1}$	(Bielsky et al., 1985)
$k_{12} = 7.0\times10^9 M^{-1}s^{-1}$	(Beck, 1969)
$k_{13} = 6.6\times10^9 M^{-1}s^{-1}$	(Laat and Gellard, 1999)
$pk_a = 11.6$	(Perry et al., 1981)

3.1.3 Acid-base Conjugate Equilibrium

Hydrogen peroxide dissociates in water as follows:

$$H_2O_2 \xleftrightarrow{k_a} H^+ + HO_2^- \qquad k_a = \frac{[H^+][HO_2^-]}{[H_2O_2]} \qquad \text{(R16)}$$

Thus, H_2O_2 and HO_2^- are a pair of conjugate acid and base, and they are related through the equilibrium equation above.

The exact concentration of hydrogen peroxide can be calculated using the equilibrium equation of reaction (R16) as follows:

$$[H_2O_2] = k_a^{-1}.[HO_2^-][H^+] \tag{3.2}$$

The total concentration of the species at equilibrium [C_{tot}] is expressed as:

$$[C_{tot}] = [H_2O_2] + [HO_2^-] \tag{3.3}$$

Hence, the new equilibrium concentrations for the individual species can now be calculated from the total mole equation:

$$[H_2O_2] = \frac{[C_{tot}]}{1 + k_a.[H^+]^{-1}} \tag{3.4}$$

$$[HO_2^-] = \frac{[C_{tot}]}{1 + k_a^{-1}.[H^+]} \tag{3.5}$$

3.2 Kinetic Model Development for Phenol Degradation by UV/H_2O_2 System

3.2.1 Completely Mixed Batch Reactor (CMBR)

Knowledge of the kinetic parameters of the photochemical reactions for organic pollutants is important in order to select and optimize an appropriate UV treatment technology. In this study, a kinetic model has been developed for phenol degradation in a UV/H_2O_2 system. First, it is assumed that the reactions are isothermal at 27°C and that they obey the reaction mechanism R1 to R15. The model is based on a molar balance of the species involved in the reactions. The kinetic rate expressions can be written for the species of interest which are: H_2O_2 / HO_2^-, $^{\bullet}OH$, $HO_2^{\bullet}$, $O_2^{\bullet -}$, and C_6H_5OH.

As explained in 3.1.3, H_2O_2 and HO_2^- are acid-base conjugates. Although the reactions of the UV/H_2O_2 oxidation process are fast reactions, equilibrium processes do take place and have to be taken into account. Based on the rapid equilibrium assumption (Jordan, 1999), the species that have acid-base chemistry will develop immediate equilibrium concentrations as the oxidation reactions progress. Therefore, the model has to be formulated in a way that resolves this chemical equilibrium.

Writing the mole balance for the total concentration of H_2O_2 and HO_2^-, gives:

$$\left(-\frac{d[H_2O_2]}{dt}\right)+\left(-\frac{d[HO_2^-]}{dt}\right)=-\frac{d[C_{tot}]}{dt}=k_1[H_2O_2]+k_2[H_2O_2][^{\bullet}OH]+k_3[^{\bullet}OH]HO_2^-] \\ +k_4[H_2O_2][HO_2^{\bullet}]+k_5[H_2O_2][O_2^{\bullet-}]-k_8[^{\bullet}OH]^2-k_{10}[HO_2^{\bullet}]^2-k_{11}[HO_2^{\bullet}][O_2^{\bullet-}] \quad (3.6)$$

Based on the above mole balance on the total concentration of H_2O_2 and HO_2^-, and by using equations (3.4) and (3.5), separate model equations for H_2O_2 and HO_2^-, considering the equilibrium are modified as follows:

$$-\frac{d[H_2O_2]}{dt}=\frac{-\frac{d[C_{tot}]}{dt}}{1+k_a[H^+]^{-1}}= \\ \left(\frac{1}{1+k_a[H^+]^{-1}}\right)\begin{pmatrix}k_1[H_2O_2]+k_2[H_2O_2][^{\bullet}OH]+k_3[^{\bullet}OH]HO_2^-]+k_4[H_2O_2][HO_2^{\bullet}] \\ +k_5[H_2O_2][O_2^{\bullet-}]-k_8[^{\bullet}OH]^2-k_{10}[HO_2^{\bullet}]^2-k_{11}[HO_2^{\bullet}][O_2^{\bullet-}]\end{pmatrix} \quad (3.7)$$

$$-\frac{d[HO_2^-]}{dt}=\frac{-\frac{d[C_{tot}]}{dt}}{1+k_a^{-1}[H^+]}= \\ \left(\frac{1}{1+k_a^{-1}[H^+]}\right)\begin{pmatrix}k_1[H_2O_2]+k_2[H_2O_2][^{\bullet}OH]+k_3[^{\bullet}OH]HO_2^-]+k_4[H_2O_2][HO_2^{\bullet}] \\ +k_5[H_2O_2][O_2^{\bullet-}]-k_8[^{\bullet}OH]^2-k_{10}[HO_2^{\bullet}]^2-k_{11}[HO_2^{\bullet}][O_2^{\bullet-}]\end{pmatrix} \quad (3.8)$$

It is assumed that pH is constant throughout the reactions. Since the overall accuracy of the model presented is limited by the lack of clear knowledge of some aspects of the system, such as unknown chemical composition of the treated water, the addition of pH changes is inappropriate.

Writing mole balances for remaining species gives:

$$-\frac{d[^{\bullet}OH]}{dt} = -2k_1[H_2O_2] + k_2[H_2O_2][^{\bullet}OH] + k_3[^{\bullet}OH][HO_2^-] - k_4[H_2O_2][HO_2^{\bullet}] \\ -k_5[H_2O_2][O_2^{\bullet-}] + k_8[^{\bullet}OH]^2 + k_9[^{\bullet}OH][HO_2^{\bullet}] + k_{12}[^{\bullet}OH][O_2^{\bullet-}] + k_{13}[C_6H_5OH][^{\bullet}OH] \quad (3.9)$$

$$-\frac{d[HO_2^{\bullet}]}{dt} = -k_2[H_2O_2][^{\bullet}OH] - k_3[^{\bullet}OH][HO_2^-] + k_4[H_2O_2][HO_2^{\bullet}] \\ -k_6[O_2^{\bullet-}][H^+] + k_7[HO_2^{\bullet}] + k_9[^{\bullet}OH][HO_2^{\bullet}] + k_{10}[HO_2^{\bullet}]^2 + k_{11}[HO_2^{\bullet}][O_2^{\bullet-}] \quad (3.10)$$

$$-\frac{d[O_2^{\bullet-}]}{dt} = k_5[H_2O_2][O_2^{\bullet-}] + k_6[O_2^{\bullet-}][H^+] - k_7[HO_2^{\bullet}] + k_{11}[HO_2^{\bullet}][O_2^{\bullet-}] + k_{12}[^{\bullet}OH][O_2^{\bullet-}] \quad (3.11)$$

$$-\frac{d[C_6H_5OH]}{dt} = k_{20}[C_6H_5OH] + k_{13}[C_6H_5OH][OH^{\bullet}] \quad (3.12)$$

The mole balance for each species X_i in a CMBR yields a set of ordinary differential equations in the form:

$$\frac{dX_i}{dt} = -r_i, \qquad X_i|_{t=0} = X_{i0} \quad (3.13)$$

Where X_{i0} and r_i are the initial concentration and the overall kinetic rate expression for species *i*, respectively. The model species along with the corresponding variables X_i are presented in Table 3.2. It should be noted that X_1-X_6 are used in the kinetic model. X_7 and X_8 are the intermediates and will be used in determination of the corresponding rate

constants (3.33)-(3.40). Since 1,3-dihydroxybenzene is produced in negligible amounts, it is not taken into account.

Table 3.2: Notations used for the reaction components

Compound/ parameter	Variable Used
H_2O_2	X_1
HO_2^-	X_2
$\dot{O}H$	X_3
$HO_2^{\bullet}$	X_4
$O_2^{\bullet -}$	X_5
Phenol	X_6
1,2- dihydroxybenzene	X_7
1,4- dihydroxybenzene	X_8

Using the notation in Table 3.2, equations (3.7)-(3.12) are rewritten as:

$$\frac{dX_1}{dt} = \left(\frac{1}{1+10^{-11.6+pH}}\right)\left(-\left(\phi_1 I_0\left(\frac{\varepsilon_1 X_1 + \varepsilon_2 X_2}{\varepsilon_1 X_1 + \varepsilon_2 X_2 + \varepsilon_6 X_6}\right)\times \left(1-\exp(-2.303b(\varepsilon_1 X_1 + \varepsilon_2 X_2 + \varepsilon_6 X_6))\right)\right) - k_2 X_1 X_3\right) - k_3 X_2 X_3 - k_4 X_1 X_4 - k_5 X_1 X_5 + k_8 X_3^2 + k_{10} X_4^2 + k_{11} X_4 X_5 \quad (3.14)$$

$$\frac{dX_2}{dt} = \left(\frac{1}{1+10^{11.6-pH}}\right)\left(-\left(\phi_1 I_0\left(\frac{\varepsilon_1 X_1 + \varepsilon_2 X_2}{\varepsilon_1 X_1 + \varepsilon_2 X_2 + \varepsilon_6 X_6}\right)\times \left(1-\exp(-2.303b(\varepsilon_1 X_1 + \varepsilon_2 X_2 + \varepsilon_6 X_6))\right)\right) - k_2 X_1 X_3\right) - k_3 X_2 X_3 - k_4 X_1 X_4 - k_5 X_1 X_5 + k_8 X_3^2 + k_{10} X_4^2 + k_{11} X_4 X_5 \quad (3.15)$$

$$\frac{dX_3}{dt} = 2\left(\phi_1 I_0\left(\frac{\varepsilon_1 X_1 + \varepsilon_2 X_2}{\varepsilon_1 X_1 + \varepsilon_2 X_2 + \varepsilon_6 X_6}\right)\times \left(1-\exp(-2.303b(\varepsilon_1 X_1 + \varepsilon_2 X_2 + \varepsilon_6 X_6))\right)\right) - k_2 X_1 X_3 - k_3 X_2 X_3 + k_4 X_1 X_4 + k_5 X_1 X_5 - k_8 X_3^2 - k_9 X_3 X_4 - k_{12} X_3 X_5 - k_{13} X_3 X_6 \quad (3.16)$$

$$\frac{dX_4}{dt} = k_2 X_1 X_3 + k_3 X_2 X_3 - k_4 X_1 X_4 + 10^{-pH}.k_6 X_5 - k_7 X_4 - k_9 X_3 X_4 - k_{10} X_4^2 - k_{11} X_4 X_5 \quad (3.17)$$

$$\frac{dX_5}{dt} = -k_5 X_1 X_5 - 10^{-pH}.k_6 X_5 + k_7 X_4 - k_{11} X_4 X_5 - k_{12} X_3 X_5 \quad (3.18)$$

$$\frac{dX_6}{dt} = -\left(\phi_2 I_0 \left(\frac{\varepsilon_6 X_6}{(1-\exp(-2.303(b\varepsilon_1 X_1 + \varepsilon_2 X_2 + \varepsilon_6 X_6)))} \right) \right) - k_{13} X_6 X_3 \quad (3.19)$$

Table 3.3 shows the photolysis parameters used in the model.

Table 3.3 : Notations used for photolysis parameters

Parameter	Variable Used
Quantum yields of H_2O_2 and HO_2^-, ($\phi_{H_2O_2}$, $\phi_{HO_2^-}$)	ϕ_1
Quantum yield of phenol, (ϕ_{phenol})	ϕ_2
Molar Extinction coefficient of phenol, (ε_{phenol})	ε_6
Molar Extinction coefficient of H_2O_2, ($\varepsilon_{H_2O_2}$)	ε_1
Molar Extinction coefficient of HO_2^-, ($\varepsilon_{HO_2^-}$)	ε_2
UV pathlength	b

Equations (3.14)-(3.19) are a set of stiff ordinary differential equations. In order to simulate the reactions, the model was solved using the Matlab built-in function Ode15s, which is employing an implicit method. Ode15s is a multi-step solver based on the numerical differentiation formulas (NDFs).

An initial value ordinary differential equations (ODE) problem is shown as follows:

$$\frac{dy}{dt} = f(\mathbf{y}) \ , \ \mathbf{y}\big|_{t=0} = \mathbf{y}_0 \tag{3.20}$$

Numerical techniques are used for solving this equation involve starting at the initial condition and stepping along the x-axis. At each step, a new value of y is estimated. As more steps are taken, the form of the required solution y(t) is determined. In single-step algorithms information of y_i and $f(t_i, y_i)$ is used to approximate the function y at the next time step, hence the value y_{i+1} is obtained from the following equation:

$$(\mathbf{y}_{i+1} - \mathbf{y}_i)/h = F(f, \mathbf{t}_i, \mathbf{t}_{i+1}, \mathbf{y}_{i+1}, \mathbf{y}_i) \tag{3.21}$$

If y_{i+1} is absent, such algorithms are *explicit* and if y_{i+1} is present, such algorithms are called *implicit* and some form of root-finding must be used to derive y_{i+1} .

In multi-step algorithms information from m past steps are employed to calculate y_{i+1} :

$$y_{i+1} = \sum_{k=1}^{m} \alpha_k y_{i+1-k} + h \sum_{k=1}^{m} \beta_k f(t_{i+1-k}, y_{i+1-k}) \tag{3.22}$$

Again, when $\beta_0 \neq 0$, algorithms are implicit. When $\beta_0 = 0$, the algorithm is explicit.

Stiff ode problem occurs when the solution to the system of equations contains components with widely different "time scales". For instance when one term decays much more faster than the other one:

$$y = Ae^{-t} + Be^{-100t} \tag{3.23}$$

Traditional methods are unable to produce reliable solutions to these problems. Implicit multi-step algorithms are more accurate and more stable than explicit multi-step algorithms, and they are best suited to solve stiff initial value odes.

In the reaction system, H_2O_2, $HO^{\cdot}_2$, and phenol are light-absorbing species. Table 3.4 gives the numerical values of the extinction coefficients and quantum yields.

Table 3.4: Numerical values of the photolysis parameters

Kinetic Parameter	Numerical Value/ Unit	References
$\phi_{H_2O_2}$	0.5	Crittenden et al.,1999
$\phi_{HO_2^-}$	0.5	Crittenden et al.,1999
ϕ_{phenol}	0.12	Ho et al., 1996
ε_{phenol}	51600 $m^{-1} M^{-1}$	Gimeno et al.,2005
$\varepsilon_{H_2O_2}$	1800 $m^{-1} M^{-1}$	Crittenden et al.,1999
$\varepsilon_{HO_2^-}$	22800 $m^{-1} M^{-1}$	Crittenden et al.,1999

Experimental data collected from literature were used to validate the model (3.14)-(3.19). Alnaizy and Akgerman (2000) conducted a set of experiments in a batch cylindrical photoreactor (Table 3.5). A photoreactor can be operated at different hydrogen peroxide concentrations. Let R denote the ratio of hydrogen peroxide concentration to that of phenol. The reactor efficiency for different values of R was evaluated. Kinetic parameters used in the simulations are listed in Table 3.4.

Table 3.5: Operational conditions and reactor data used in the simulation,by Alnaizy and Akgerman (2000)

Reactor specification	Numerical value
Volume	310 mL
Diameter	65 mm
Reflection Factor[1]	1
Lighted Length	63.5 mm
Quartz Diameter	9.5 mm
Radiation Wavelength	254 nm
Power	15 W
UV Irradiation Rate	1.516×10^{-6} $E.L^{-1}.s^{-1}$

[1] Reflection factor is defined as the proportion of incident flux that is reflected by a surface. Here, reflection factor of 1 means all the UV irradiation remains in the reactor.

Figure 3.3 presents plots of three simulation cases. The first case has H_2O_2 /phenol ratio of 495 at 27°C and initial phenol concentration of 2.23×10^{-3}M. Keeping the H_2O_2 /phenol ratio at 200 with a temperature of 27°C, two other simulation runs were generated with initial phenol concentrations of 0.43×10^{-3} and $0.25\times10^{-3}M$, respectively. Figure 3.3 also compares the simulation results with experimental data obtained from Alnaizy and Akgerman (2000) for phenol oxidation in UV/H_2O_2 at the same reactor conditions. In this study, experimental data points were accurately collected from plots in literature using a digitizer software. Figure 3.4 shows the Residual diagram comparing the errors for different initial concentrations. It can be observed from this figure that no specific pattern of error exists for this model. Figure 3.5 shows the predicted concentrations plotted versus the experimental data. The values of R-squared are shown on the graph. R-squared is a descriptive measure between 0 and 1 which shows the relative predictive power of a model. The closer it is to one, the model has greater ability to predict. It is calculated through the following equation:

$$R^2 = 1 - \frac{\sum (y_i - \hat{y}_i)^2}{\sum (y_i)^2 - \frac{(\sum y_i)^2}{n}} \tag{3.24}$$

Figure 3.3, Figure 3.4, and Figure 3.5 show that the kinetic model predictions of phenol concentration are in good agreement with the experimental data.

Another set of plots (Figure 3.6) show free radicals concentrations variations during the reactions. The plots show the prediction of free radicals concentration in a UV/H_2O_2 system, for an initial phenol concentration of 0.00043 M and a H_2O_2 /phenol ratio of 200. Figure 3.6 shows that as the reactions start, concentration of free radicals increases from zero to an almost constant amount within about 20 minutes, where phenol has been fully degraded within this time period (second case, Figure 3.3).

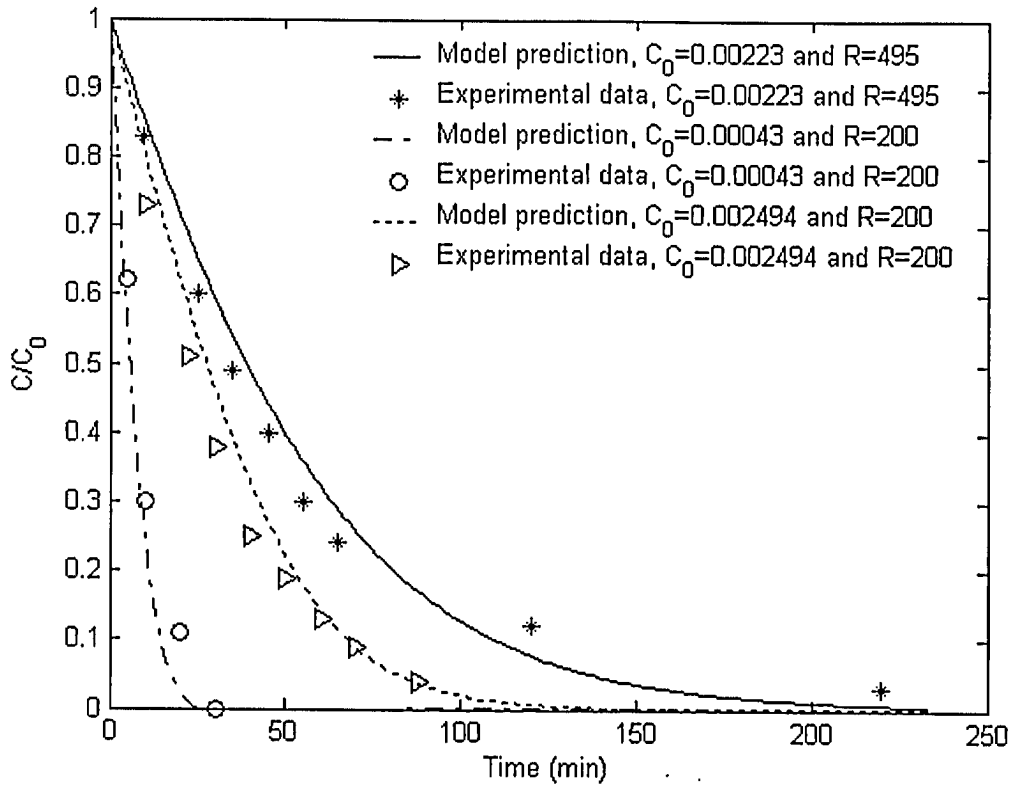

Figure 3.3: Comparison of model predictions with data in a batch photolysis reactor (Data source: Alnaizy and Akgerman, 2000)

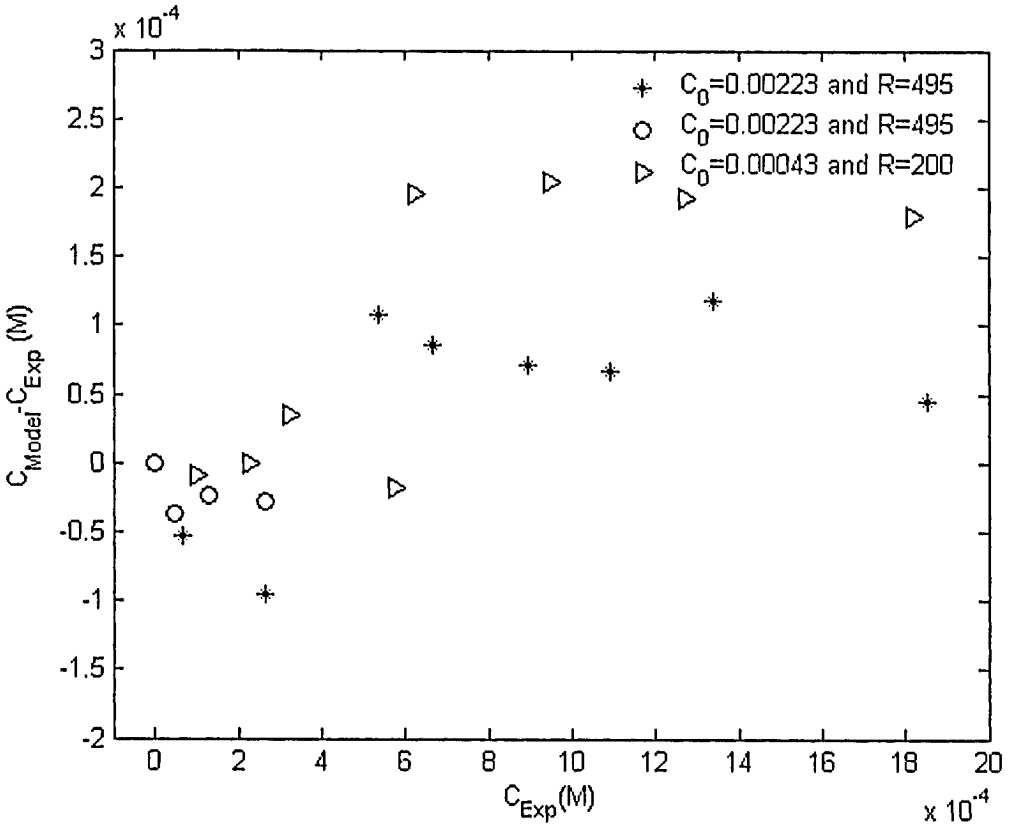

Figure 3.4: Residual diagram for model validation, No similar pattern observed

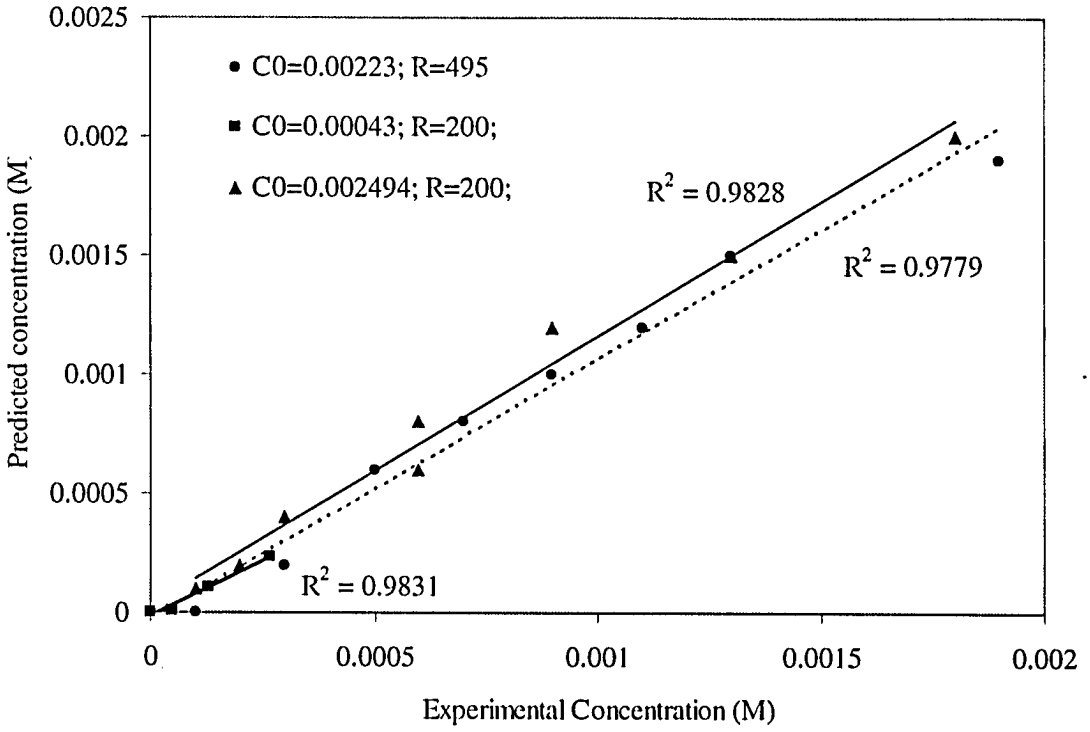

Figure 3.5: Predicted data versus experimental data, with the R-squared values shown for each set of data.

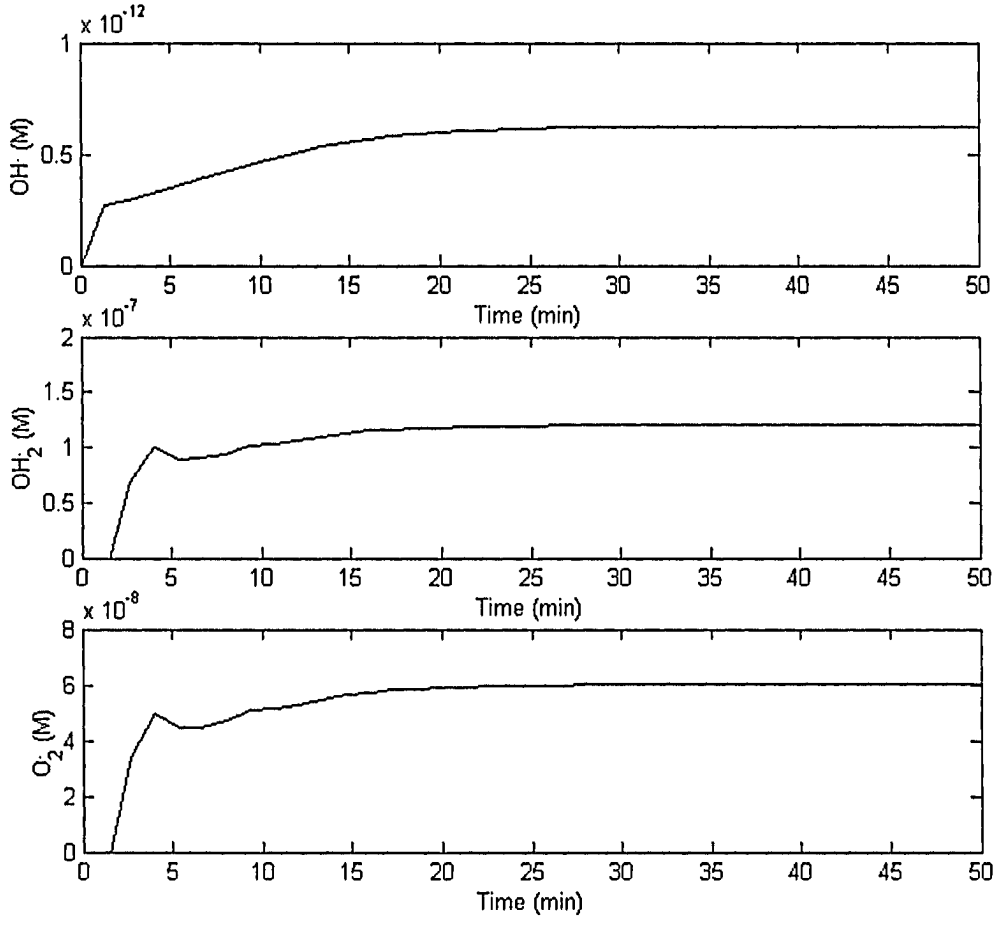

Figure 3.6: Free radicals concentrations during the reactions in CMBR, with C_0=0.00043 M and initial molar H_2O_2/phenol ratio of 200, pH buffered at 7 and 27°C.

3.2.2 CMBR Model with Intermediates

Noting that the by-products of phenol oxidation react with the hydroxyl radicals according to a second order kinetics, two more equations representing the molar balances of 1,2- and 1,4- dihydroxybenzene were added to the molar balance (3.7)-(3.12). Considering the two intermediates, terms were added to the molar balances of hydroxyl radical and phenol, equations (3.9) and (3.12). Since reactions of 1,2- and 1,4-dihydroxybenzene do not involve $[H_2O_2]$, $[HO_2^-]$, $[HO_2^\bullet]$, and $[O_2^{\bullet-}]$, the molar balances of these components remain unchanged. The following molar balances were obtained for the system with 1,2- and 1,4- dihydroxybenzene considered:

$$-\frac{d[H_2O_2]}{dt}=\frac{-\frac{d[C_{tot}]}{dt}}{1+k_a[H^+]^{-1}}=\left(\frac{1}{1+k_a[H^+]^{-1}}\right)\begin{pmatrix}k_1[H_2O_2]+k_2[H_2O_2][^\bullet OH]+k_3[^\bullet OH][HO_2^-]\\+k_4[H_2O_2][HO_2^\bullet]+k_5[H_2O_2][O_2^{\bullet-}]-k_8[^\bullet OH]^2\\-k_{10}[HO_2^\bullet]^2-k_{11}[HO_2^\bullet][O_2^{\bullet-}]\end{pmatrix} \tag{3.25}$$

$$-\frac{d[HO_2^-]}{dt}=\frac{-\frac{d[C_{tot}]}{dt}}{1+k_a^{-1}[H^+]}=\left(\frac{1}{1+k_a^{-1}[H^+]}\right)\begin{pmatrix}k_1[H_2O_2]+k_2[H_2O_2][^\bullet OH]+k_3[^\bullet OH][HO_2^-]\\+k_4[H_2O_2][HO_2^\bullet]+k_5[H_2O_2][O_2^{\bullet-}]-k_8[^\bullet OH]^2\\-k_{10}[HO_2^\bullet]^2-k_{11}[HO_2^\bullet][O_2^{\bullet-}]\end{pmatrix} \tag{3.26}$$

$$\begin{aligned}-\frac{d[^\bullet OH]}{dt}&=-2k_1[H_2O_2]+k_2[H_2O_2][^\bullet OH]+k_3[^\bullet OH][HO_2^-]-k_4[H_2O_2][HO_2^\bullet]\\&-k_5[H_2O_2][O_2^{\bullet-}]+k_8[^\bullet OH]^2+k_9[^\bullet OH][HO_2^\bullet]+k_{12}[^\bullet OH][O_2^{\bullet-}]+k_{14}[C_6H_5OH][OH^\bullet]\\&+k_{15}[C_6H_5OH][OH^\bullet]+k_{17}[1,2-C_6H_4(OH)_2][OH^\bullet]+k_{18}[1,4-C_6H_4(OH)_2][OH^\bullet]\end{aligned} \tag{3.27}$$

$$\begin{aligned}-\frac{d[HO_2^\bullet]}{dt}&=-k_2[H_2O_2][^\bullet OH]-k_3[^\bullet OH][HO_2^-]+k_4[H_2O_2][HO_2^\bullet]-k_6[O_2^{\bullet-}][H^+]\\&+k_7[HO_2^\bullet]+k_9[^\bullet OH][HO_2^\bullet]+k_{10}[HO_2^\bullet]^2+k_{11}[HO_2^\bullet][O_2^{\bullet-}]\end{aligned} \tag{3.28}$$

$$-\frac{d[O_2^{\bullet-}]}{dt}=k_5[H_2O_2][O_2^{\bullet-}]+k_6[O_2^{\bullet-}][H^+]-k_7[HO_2^\bullet]+k_{11}[HO_2^\bullet][O_2^{\bullet-}]+k_{12}[^\bullet OH][O_2^{\bullet-}] \tag{3.29}$$

$$-\frac{d[C_6H_5OH]}{dt} = k_{20}[C_6H_5OH] + k_{14}[C_6H_5OH][OH^\bullet] + k_{15}[C_6H_5OH][OH^\bullet] \tag{3.30}$$

$$-\frac{d[1,2-C_6H_4(OH)_2]}{dt} = -k_{14}[C_6H_5OH][OH^\bullet] + k_{17}[1,2-C_6H_4(OH)_2][OH^\bullet] \tag{3.31}$$

$$-\frac{d[1,4-C_6H_4(OH)_2]}{dt} = -k_{15}[C_6H_5OH][OH^\bullet] + k_{18}[1,4-C_6H_4(OH)_2][OH^\bullet] \tag{3.32}$$

Using symbols in Table 3.2, the model is rewritten:

$$\frac{dX_1}{dt} = \left(\frac{1}{1+10^{-11.6+pH}}\right)\left(-\left(\phi_1 I_0\left(\frac{\varepsilon_1 X_1 + \varepsilon_2 X_2}{\varepsilon_1 X_1 + \varepsilon_2 X_2 + \varepsilon_6 X_6}\right)\times \left(1-\exp(-2.303b(\varepsilon_1 X_1 + \varepsilon_2 X_2 + \varepsilon_6 X_6))\right)\right) - k_2 X_1 X_3 - k_3 X_2 X_3 - k_4 X_1 X_4 - k_5 X_1 X_5 + k_8 X_3^2 + k_{10} X_4^2 + k_{11} X_4 X_5\right) \tag{3.33}$$

$$\frac{dX_2}{dt} = \left(\frac{1}{1+10^{11.6-pH}}\right)\left(-\left(\phi_1 I_0\left(\frac{\varepsilon_1 X_1 + \varepsilon_2 X_2}{\varepsilon_1 X_1 + \varepsilon_2 X_2 + \varepsilon_6 X_6}\right)\times \left(1-\exp(-2.303b(\varepsilon_1 X_1 + \varepsilon_2 X_2 + \varepsilon_6 X_6))\right)\right) - k_2 X_1 X_3 - k_3 X_2 X_3 - k_4 X_1 X_4 - k_5 X_1 X_5 + k_8 X_3^2 + k_{10} X_4^2 + k_{11} X_4 X_5\right) \tag{3.34}$$

$$\frac{dX_3}{dt} = 2\left(\phi_1 I_0\left(\frac{\varepsilon_1 X_1 + \varepsilon_2 X_2}{\varepsilon_1 X_1 + \varepsilon_2 X_2 + \varepsilon_6 X_6}\right)\times \left(1-\exp(-2.303b(\varepsilon_1 X_1 + \varepsilon_2 X_2 + \varepsilon_6 X_6))\right)\right) - k_2 X_1 X_3 - k_3 X_2 X_3 + k_4 X_1 X_4 + k_5 X_1 X_5 - k_8 X_3^2 - k_9 X_3 X_4 - k_{12} X_3 X_5 - k_{14} X_3 X_6 - k_{15} X_3 X_6 - k_{17} X_3 X_7 - k_{18} X_3 X_8 \tag{3.35}$$

$$\frac{dX_4}{dt} = k_2 X_1 X_3 + k_3 X_2 X_3 - k_4 X_1 X_4 + 10^{-pH} . k_6 X_5 - k_7 X_4 - k_9 X_3 X_4 - k_{10} X_4^2 - k_{11} X_4 X_5 \tag{3.36}$$

$$\frac{dX_5}{dt} = -k_5 X_1 X_5 - 10^{-pH} . k_6 X_5 + k_7 X_4 - k_{11} X_4 X_5 - k_{12} X_3 X_5 \tag{3.37}$$

$$\frac{dX_6}{dt} = -\left(\phi_2 I_0 \left(\frac{\varepsilon_6 X_6}{\varepsilon_1 X_1 + \varepsilon_2 X_2 + \varepsilon_6 X_6} \right) \left(1 - \exp(-2.303(b\varepsilon_1 X_1 + \varepsilon_2 X_2 + \varepsilon_6 X_6))\right) \right) \tag{3.38}$$
$$- k_{14} X_6 X_3 - k_{15} X_6 X_3$$

$$\frac{dX_7}{dt} = k_{14} X_3 X_6 - k_{17} X_3 X_7 \tag{3.39}$$

$$\frac{dX_8}{dt} = k_{15} X_3 X_6 - k_{18} X_3 X_8 \tag{3.40}$$

As stated earlier in Section 3.1.2, values of k reported in the literature so far are based on specific experimental results and are reliable only for the associated set-up and concentrations. As such, the results may not be generalized to other systems. Using values of the rate constants (k_{14}, k_{15}, k_{17}, and k_{18}) as reported by Alnaizy and Akgerman (2000), the simulation results are presented in Figure 3.8. Figure 3.8 shows model prediction and data of phenol concentration and the two major intermediates concentrations (Catechol and Hydroquinone).

In this study, the rate constants k_{14}, k_{15}, k_{17}, and k_{18} are estimated through a nonlinear least square objective function, so that the model prediction are as close as possible to experimental data (Figure 3.9).

The objective function for minimizing the error between the model prediction and the experimental values is defined by:

minimize:

$$f = \sum (X_{6,predicted} - X_{6,experiment})^2 + (X_{7,predicted} - X_{7,experiment})^2 + (X_{8,predicted} - X_{8,experiment})^2$$

Subject to: $\frac{dX_i}{dt} = r_i \quad (i = 1:8)$ (3.41)

$$k_{14}, k_{15}, k_{17}, k_{18} > 0$$

The optimum values have been determined to be:

$$k_{14} = 0.9 \times 10^9 \, M^{-1}s^{-1} \tag{3.42}$$

$$k_{15} = 0.2 \times 10^9 \, M^{-1}s^{-1} \tag{3.43}$$

$$k_{17} = 0.9 \times 10^9 \, M^{-1}s^{-1} \tag{3.44}$$

$$k_{18} = 0.8 \times 10^8 \, M^{-1}s^{-1} \tag{3.45}$$

3.2.3 Continuous Stirred Tank Reactor (CSTR)

Batch treatment is suitable only for photochemical treatment in small reactors. Excessive pumping and mixing requirements make large batch reactors impractical and several cycles for each reactor increases manual operating costs, whereas automation decreases operating cost at the expense of capital cost. For a CSTR model, the inlet and outlet flow rates along with the rate equations should be added. A schematic diagram of a CSTR is given in Figure 3.7 :

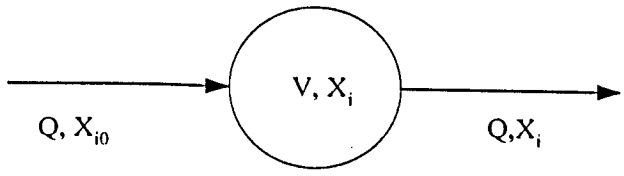

Figure 3.7: Schematic diagram of a continuous flow reactor

The general mole balance of species *i* is:

$$\text{Accumulation} = \text{Inflow} - \text{Outflow} + \text{Production rate} \tag{3.46}$$

$$\frac{dX_i}{dt}V = QX_{i0} - QX_i + Vr_i \tag{3.47}$$

Since all considered components are soluble, the model differential equations are generally stated as:

$$\frac{dX_i}{dt} = \frac{Q(X_{i0} - X_i)}{V} + r_i, \qquad X_i\big|_{t=0} = X_{i0} \tag{3.48}$$

where Q is the inlet flow rate to the reactor (L. s^{-1}) and V is the reactor volume (L).

X_{i0} is the inlet concentration of species i and also is the concentration of compound i in the reactor at time zero (initial conditions). Equation (3.48) is expanded into a set of ODEs to be solved simultaneously.

$$\frac{dX_1}{dt} = \frac{Q(X_{1,0} - X_1)}{V} + \left(\frac{1}{1+10^{-11.6+pH}}\right)\left(\begin{array}{l} -\left(\phi_1 I_0\left(\dfrac{\varepsilon_1 X_1 + \varepsilon_2 X_2}{\varepsilon_1 X_1 + \varepsilon_2 X_2 + \varepsilon_6 X_6}\right)\times \right. \\ \qquad \left.(1-\exp(-2.303b(\varepsilon_1 X_1 + \varepsilon_2 X_2 + \varepsilon_6 X_6)))\right) \\ -k_2 X_1 X_3 - k_3 X_2 X_3 - k_4 X_1 X_4 - k_5 X_1 X_5 + k_8 X_3^2 \\ +k_{10} X_4^2 + k_{11} X_4 X_5 \end{array}\right) \tag{3.49}$$

$$\frac{dX_2}{dt} = \frac{Q(X_{2,0} - X_2)}{V} + \left(\frac{1}{1+10^{11.6-pH}}\right)\left(\begin{array}{l} -\left(\phi_1 I_0\left(\dfrac{\varepsilon_1 X_1 + \varepsilon_2 X_2}{\varepsilon_1 X_1 + \varepsilon_2 X_2 + \varepsilon_6 X_6}\right)\times \right. \\ \qquad \left.(1-\exp(-2.303b(\varepsilon_1 X_1 + \varepsilon_2 X_2 + \varepsilon_6 X_6)))\right) \\ -k_2 X_1 X_3 - k_3 X_2 X_3 - k_4 X_1 X_4 - k_5 X_1 X_5 + k_8 X_3^2 \\ +k_{10} X_4^2 + k_{11} X_4 X_5 \end{array}\right) \tag{3.50}$$

$$\frac{dX_3}{dt}=\frac{Q(X_{3,0}-X_3)}{V}+2\left(\phi_1 I_0\left(\frac{\varepsilon_1 X_1+\varepsilon_2 X_2}{\varepsilon_1 X_1+\varepsilon_2 X_2+\varepsilon_6 X_6}\right)\times \left(1-\exp(-2.303b(\varepsilon_1 X_1+\varepsilon_2 X_2+\varepsilon_6 X_6))\right)\right)-k_2 X_1 X_3-k_3 X_2 X_3 + k_4 X_1 X_4+k_5 X_1 X_5-k_8 X_3^2-k_9 X_3 X_4-k_{12} X_3 X_5-k_{13} X_3 X_6 \quad (3.51)$$

$$\frac{dX_4}{dt}=\frac{Q(X_{4,0}-X_4)}{V}+k_2 X_1 X_3+k_3 X_2 X_3-k_4 X_1 X_4+10^{-pH}.k_6 X_5-k_7 X_4-k_9 X_3 X_4 -k_{10} X_4^2-k_{11} X_4 X_5 \quad (3.52)$$

$$\frac{dX_5}{dt}=\frac{Q(X_{5,0}-X_5)}{V}-k_5 X_1 X_5-10^{-pH}.k_6 X_5+k_7 X_4-k_{11} X_4 X_5-k_{12} X_3 X_5 \quad (3.53)$$

$$\frac{dX_6}{dt}=\frac{Q(X_{6,0}-X_6)}{V}-\left(\phi_2 I_0\left(\frac{\varepsilon_6 X_6}{\varepsilon_1 X_1+\varepsilon_2 X_2+\varepsilon_6 X_6}\right)\left(1-\exp(-2.303(b\varepsilon_1 X_1+\varepsilon_2 X_2+\varepsilon_6 X_6))\right)\right)-k_{13} X_6 X_3 \quad (3.54)$$

Initial conditions to solve the differential equations are provided in Table 3.6. In Table 3.6, R is the ratio of initial total concentration of hydrogen peroxide species [C_{tot}], to that of phenol C_0, i.e.: [C_{tot}] = R×C_0. As it is discussed in Section 3.1.3, rapid equilibrium happens immediately after the addition of hydrogen peroxide to the solution. Hydrogen peroxide partially dissociates to HO_2^-. Using equations (3.4) and (3.5), the initial concentrations of the acid-base conjugate species, HO_2^- and H_2O_2 will be calculated as follows:

$$[H_2O_2]=\frac{\mathrm{R\,C_0}}{1+k_a.[H^+]^{-1}} \quad (3.55)$$

$$[HO_2^-] = \frac{R C_0}{1 + k_a^{-1}.[H^+]} \tag{3.56}$$

Table 3.6: Components' initial concentrations

Compound	Dummy Variables (Matlab)	Initial Concentration (M)
H_2O_2	X_1	$RC_0 / (1+10^{-11.6+pH})$ R= 0 to 10^3 RC_0=0 to 10
HO_2^-	X_2	$RC_0 / (1+10^{11.6-pH})$ R= 0 to 10^3 RC_0=0 to 10
$OH^\bullet$	X_3	0
$HO_2^\bullet$	X_4	0
$O_2^{\bullet -}$	X_5	0
C_6H_5OH	X_6	C_0 $C_0=10^{-5}$ to 10^{-2}

3.3 Concluding Remarks

In this chapter a reaction mechanism for phenol degradation in UV/H_2O_2 system was proposed. By means of the proposed reaction mechanism, a kinetic model for the UV/H_2O_2 system was developed and validated. Also reaction rate constants for phenol oxidation intermediates were evaluated using a nonlinear least square objective function. In the next chapter the biological model employed from literature to obtain the overall combined photochemical-biological model is introduced.

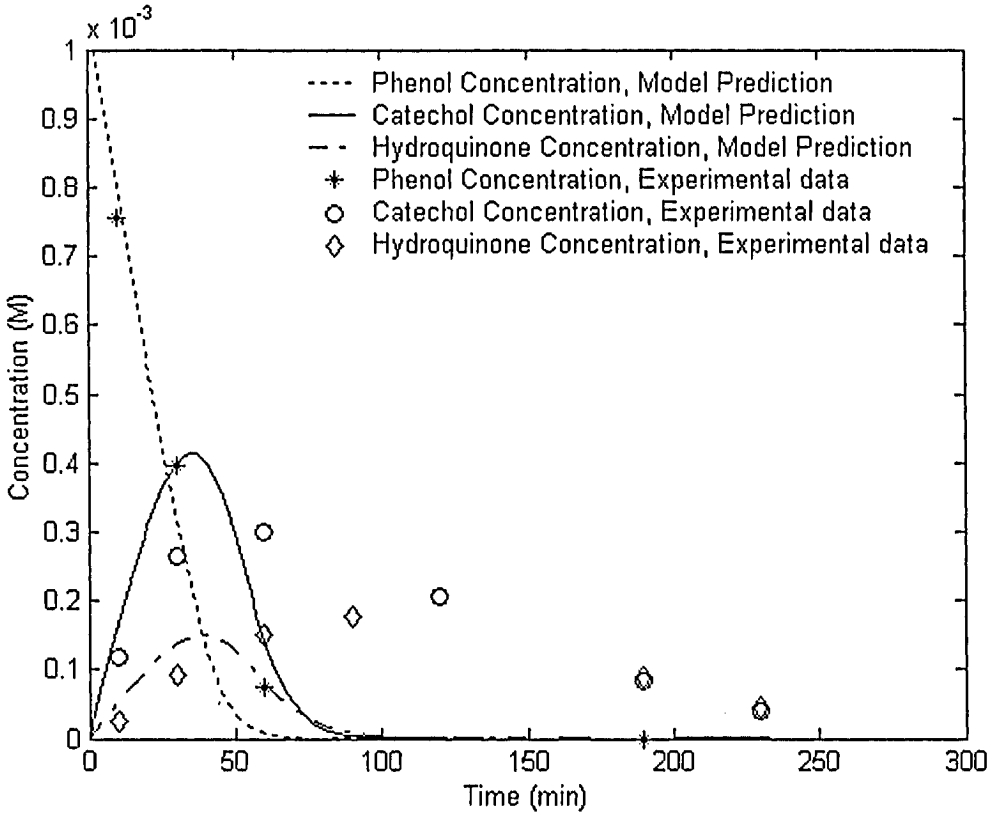

Figure 3.8: Simulation results for the UV/ H_2O_2 CMBR using the reaction rates presented by Alnaizy and Akgerman (2000), where $C_{0,ph}$=0.00107 M and H_2O_2/phenol ratio of 45, T=27°C.

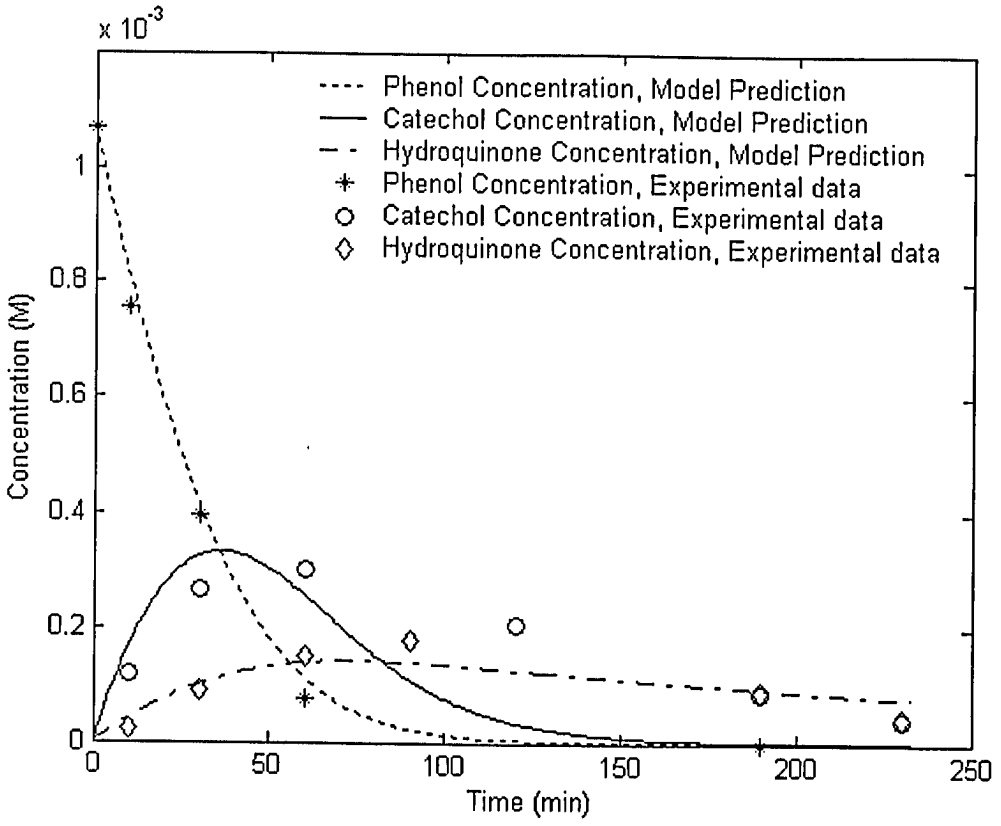

Figure 3.9: Simulation results for the UV/ H_2O_2 CMBR using optimal estimates for k_{14},k_{15},k_{17}, and k_{18}, where $C_{0,ph}$=0.00107 M and H_2O_2/phenol ratio of 45, T=27°C.

CHAPTER 4
PHENOL BIODEGRADATION KINETIC MODEL

4.1 Biokinetic Model for Batch Reactor

Modeling is a good tool for bioreactor design and analysis. In order to develop a meaningful predictive capability, data must be fit to an appropriate kinetic model. The Monod expression is an acceptable mathematical description of experiments conducted with bacterial culture growing on single substrates (Monod, 1949) as follows:

$$\mu = \mu_{max} \frac{S}{K_S + S} \tag{4.1}$$

where μ is the microbial specific growth rate (h^{-1}), and K_s, the half saturation constant (mg/L), is defined as the substrate concentration at which μ is equal to half μ_{max}. In other words, K_s value shows the attraction of the microorganisms to the substrate.

The microbial specific rate μ is defined by:

$$\mu = \frac{1}{Z}\frac{dZ}{dt} \tag{4.2}$$

where Z is the biomass concentration (mg/L).

Using the cell yield coefficient definition, the stoichiometric relationship between the organic substrate consumed and the microorganisms produced is expressed as follows:

$$\frac{dZ}{dt} = -Y\frac{dS}{dt} \tag{4.3}$$

The cell yield coefficient Y is one of the most important parameters used in biological kinetic models. It represents the biomass produced per substrate removed. Dividing both sides of equation (4.3) by Z we get:

$$\frac{1}{Z}\frac{dZ}{dt} = -\frac{Y}{Z}\frac{dS}{dt} \tag{4.4}$$

Although the Monod equation is conventionally used to describe phenol consumption kinetics (Reardon et al., 2000), the Haldane model is preferred in case of phenol biodegradation. However, phenol biodegradation may be inhibited by the phenol molecule itself (Nuhoglu and Yalchin, 2005). Haldane kinetics is used when the compound is self inhibiting. The difference between the Haldane and the Monod models stems from the expressions they each proposed for the specific growth rate. Unlike Monod equation, Haldane model defines the specific growth rate as follows:

$$\mu = \mu_{max}\frac{S}{K_S + S + \left(S^2/K_i\right)} \tag{4.5}$$

K_i is the inhibition constant. When K_i is very large, the Haldane equation simplifies to Monod equation. A summary of the Haldane model kinetic constants as reported in different studies is shown in Table 4.1.

In simulation studies employing the Haldane model, a striking disagreement between the measured and estimated phenol concentrations was observed when the initial phenol concentration exceeds 100 mg/L (Nuhoglu and Yalchin, 2005; Rodriguez et al., 2006).

Table 4.1: Biodegradation kinetic constant values reported for phenol biodegradation

Max. phenol concentration (mg/L)	μ_{max} (h^{-1})	K_S (mg/L)	K_i (mg/L)	Y (mg/mg)	Microorganism	Reference
54	0.11	32	-	0.8	*Pseudomonas putida* F1	Kenneth et al., 2000
1450	0.143	87.45	107	0.60	Activated sludge	Nuhoglu and Yalchin, 2005
1000	0.305	36.33	129	0.65	*Pseudomonas putida* MTCC1194	Kumar et al., 2005
500	0.569	18.539	99.374	0.521	*Pseudomonas putida* NRRL 14875	Seker et al., 1997
1750	0.078	29.31	2434.7	0.571	*Bacillus brevis*	Arutchelvan et al., 2006
500	0.38	450	195	-	*Pseudomonas aeruginosa*	Oboirien et al., 2005
500	0.58	450	127	-	*Pseudomonas fluorescence*	Oboirien et al., 2005
350	0.8	1.5	188	0.7	*Acinetobacter*	Hao et al., 2001
800	0.25	300	450	0.67	Activated sludge	Vazquez et al., 2006
500	0.42	110	380	0.77	*Trichosporon cutaneum* R57	Alexievaa et al., 2004

The discrepancy of Haldane model and the actual data is attributed to the inhibitory effect of metabolic intermediates, most notably among them 2-hydroxymuconic acid semialdehyde, of phenol degradation (Wang and Loh, 1999). 2-Hydroxymuconic acid semialdehyde (denoted by 2-hmas) is also responsible for the color change to yellow in the culture medium.

Modified versions of Haldane model have been proposed based on direct integration of the initial phenol concentration in the specific growth rate expression (Nuhoglu and Yalchin, 2005; Wang and Loh, 1999). However, they are not quite accurate since the

effect of the biological intermediate is not taken into account. The most realistic model for phenol biodegradation presented so far is the two-step model which takes into account the 2-hmas and two different microbial populations (Vazquez et al., 2006). Phenol biodegradation was assumed to go through two steps. First, phenol is degraded and then it produces the metabolic intermediate which, in turn, is mineralized by another microbial population, as descried in the equations below:

$$S_1 \rightarrow Z_1 + S_2 + P_1 \tag{4.6}$$

$$S_2 \rightarrow Z_2 + P_2 \tag{4.7}$$

Where S_1 is the phenol concentration, Z_1 is the portion of biomass concentration responsible for the phenol degradation, S_2 is the concentration of the major metabolic intermediate (2-hmas), Z_2 is the fraction of the biomass growing on S_2, and P_1 and P_2 are the unknown products or metabolic intermediates. The dynamic model for phenol biodegradation in a batch reactor is as follows (Vazquez et al., 2006):

$$\frac{dZ_1}{dt} = \mu_1 Z_1 \tag{4.8}$$

$$\frac{dS_1}{dt} = \frac{-1}{Y_1}\frac{dZ_1}{dt} \tag{4.9}$$

$$\frac{dZ_2}{dt} = \mu_2 Z_2 \tag{4.10}$$

$$\frac{dS_2}{dt} = a\frac{dZ_1}{dt} - \frac{-1}{Y_2}\frac{dZ_2}{dt} \tag{4.11}$$

where α is the growth–associated constant relating the production of metabolic intermediate to the phenol consumption. It can be concluded from equation (4.11) that the generation of the metabolic intermediate S_2 depends on the conversion of phenol S_1 by the biomass Z_1. Phenol and the metabolic intermediate are considered as inhibitory substrates, where the specific growth rates μ_1 and μ_2 can be expressed by Haldane equation. Therefore, the model for phenol biodegradation in a batch reactor becomes:

$$\frac{dZ_1}{dt} = \frac{\mu_{m1} S_1}{K_{S1} + S_1 + \left(S_1^{\,2} / K_{i1}\right)} Z_1 \tag{4.12}$$

$$\frac{dS_1}{dt} = \frac{-1}{Y_1} \frac{dZ_1}{dt} \tag{4.13}$$

$$\frac{dZ_2}{dt} = \frac{\mu_{m2} S_2}{K_{S2} + S_2 + \left(S_2^{\,2} / K_{i2}\right)} Z_2 \tag{4.14}$$

$$\frac{dS_2}{dt} = a \frac{dZ_1}{dt} - \frac{-1}{Y_2} \frac{dZ_2}{dt} \tag{4.15}$$

Vazquez et al. (2006) estimated the kinetic constants for the two-step model from experimental data. Numerical values of the rate constants are shown in Table 4.2.

Table 4.2: Kinetic parameters obtained for the two-step model (Vazquez et al., 2006)

Parameter	Numerical Values
μ_{m1}	0.25 h^{-1}
k_{S1}	300 mg L^{-1}
k_{i1}	450 mg L^{-1}
Y_1	0.67
μ_{m2}	0.1 h^{-1}
k_{S2}	70 mg L^{-1}
k_{i2}	90 mg L^{-1}
Y_2	0.8
a	0.95

Figure 4.1 compares the predictions of Monod and Haldane models and the two-step Haldane model with experimental data. Experimental data were obtained from the literature (Vazquez et al., 2006). It can be concluded from Figure 4.1 that the two-step model provides the best dynamic prediction of phenol biodegradation.

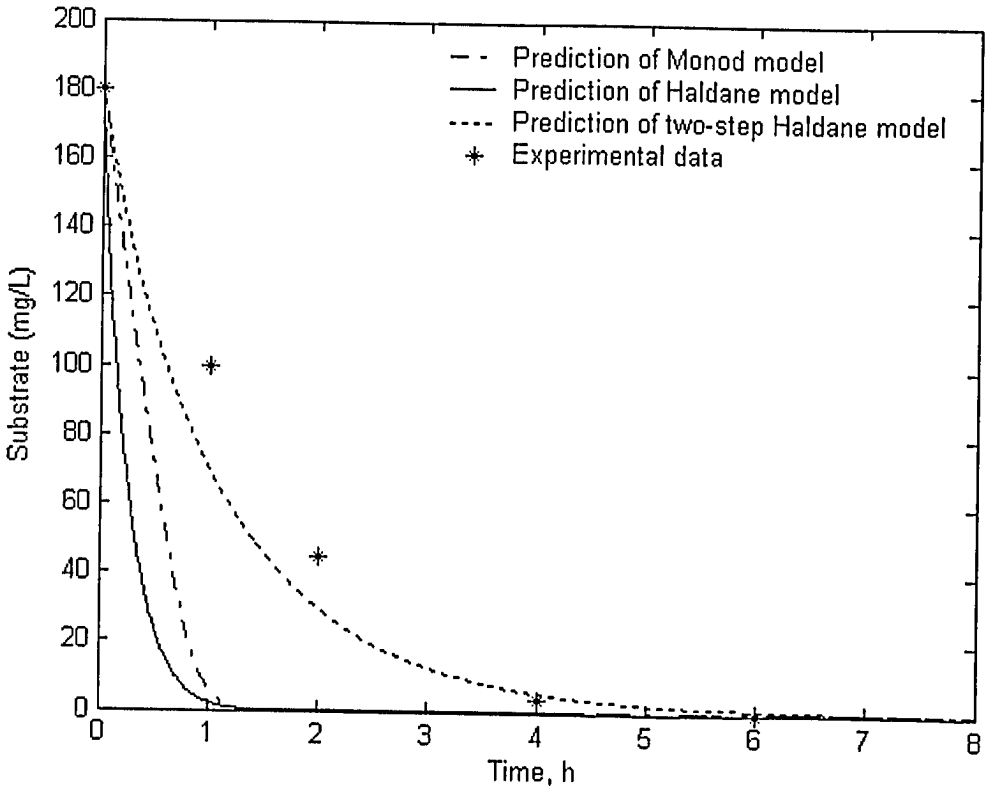

Figure 4.1: Comparison of different models prediction with experimental data for a biological batch reactor.

4.2 Biokinetic Model for Continuous Reactor

A schematic diagram of the biological CSTR with a solid settler and recycle is presented in Figure 4.2. The biomass consumes organic pollutant present in the wastewater as nutrients. The biological reactor is well mixed and aerated, and it behaves like an activated sludge. Activated sludge consists of 95% bacteria and 5% multi-cellular organisms. Allowing sufficient time for the biochemical reactions to take place, the effluent mixture is transferred to a clarifier in order to allow gravity separation of the suspended solids from the treated wastewater. The wastewater mixture just treated is separated into an effluent and a concentrated sludge. A portion of the concentrated sludge is recycled and mixed with the influent wastewater. The purpose of the activated sludge recycling is to maintain a sufficient concentration of the activated sludge in the aeration tank so that the required degree of treatment can be obtained in the desired residence time. Recycling activated sludge from the clarifier to the inlet of the aeration tank is a salient feature of the process (Metcalf and Eddy, 1991).

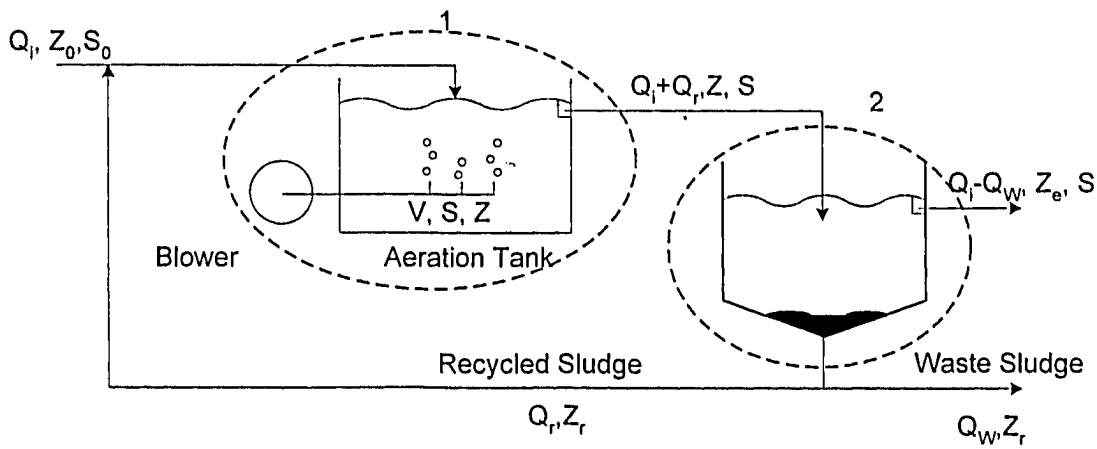

Figure 4.2: Schematic diagram of the CSTR biological reactor with a recycle

Applying a mass balance on the biomass in the CSTR, the following equation is obtained:

$$\begin{aligned}\frac{dZ}{dt}.V &= Q_i Z_0 + Q_r Z_r - (Q_i + Q_r)Z + r(Z).V \\ &= Q_i(Z_0 - Z) + Q_r(Z_r - Z) + r(Z).V\end{aligned} \tag{4.16}$$

where V is the bioreactor volume, Q_i is the inlet flow rate and Q_r is the recycled activated sludge flow rate and r(Z) represents the kinetic rate of the biomass production.

Since there is no substrate utilization or cell growth in the settling tank, the concentration ratio is proportional to the inverse of the flow rates ratio and the following relations hold:

$$\frac{Z_r}{Z} = \frac{Q_i + Q_r}{Q_r + Q_w} \tag{4.17}$$

Rearranging the equation gives:

$$Z_r - Z = \frac{Q_i - Q_w}{Q_r + Q_w} Z \tag{4.18}$$

By substituting equation (4.18) into equation (4.16) gives:

$$\frac{dZ}{dt} = \frac{Q_i}{V}(Z_0 - Z) + \frac{Q_r}{V}.\frac{Q_i - Q_w}{Q_r + Q_w}.Z + r(Z) \tag{4.19}$$

Applying a mass balance on the substrate in the CSTR gives:

$$\frac{dS}{dt} = \frac{Q_i}{V}(S_0 - S) + r(S) \tag{4.20}$$

where r(S) represents the reaction rate of the degradation of the components.

Let define the following dimensionless ratios:

$$\alpha = \frac{Q_r}{Q_i} \tag{4.21}$$

$$\gamma = \frac{Q_w}{Q_i} \tag{4.22}$$

$$\theta_B = \frac{V}{Q_i} \tag{4.23}$$

where θ_B is the retention time of wastewater in the bioreactor.

Therefore, the differential equations describing phenol biodegradation in a CSTR are re-written as:

$$\left.\frac{dZ_i}{dt}\right|_{i=1,2} = \frac{1}{\theta_B}(Z_{i0} - Z_i) + \frac{\alpha}{\theta_B}.\frac{1-\gamma}{\alpha+\gamma}.Z_i + r(Z_i) \tag{4.24}$$

$$\left.\frac{dS_i}{dt}\right|_{i=1,2} = \frac{1}{\theta_B}(S_{i0} - S_i) + r(S_i) \tag{4.25}$$

where Z_1 and Z_2 represent the biomass growing on phenol and the biomass growing on the biological intermediate, respectively. S_1 and S_2 stand for phenol and the biological intermediate, respectively.

In this study, the process to treat wastewater from phenol pollutant consists of two consecutive units. A photochemical reactor is followed by an activated sludge bioreactor unit. The latter consists of a bioreactor followed by a settling unit. The core of this study is to analyze both units and determine the best operating conditions for the whole

photochemical-biological treatment process. For designing purposes, the phenol concentration emerging from the biological unit is of major importance. Phenol amount in the stream leaving the photochemical-biological system depends on many factors: initial phenol concentration, retention time in photochemical reactor, retention time in the biological unit, and also the two ratios of recycle to inlet flow rates (α) and waste sludge flow rate to inlet flow rate (γ). Upon determining these factors, the overall photochemical-biological model should be able to predict phenol concentration in the outlet stream. Table 4.3 shows an example set of model-predicted phenol concentrations, for a practical range of α and γ (Metcalf and Eddy, 1991), for an initial phenol concentration of 0.04 M. The photochemical and biological retention times are chosen to be equal to 6 h each since the minimum treatment required for reducing phenol concentration from 0.04 to the toxic threshold for the microorganisms 0.0148 M (1400 mg/L), takes 6 h in the chemical reactor. The data presented in Table 4.3 are obtained by solving first the photochemical model (3.49)-(3.54) and then the biological model (4.24)-(4.25). The photochemical model equations (3.49)-(3.54) were solved for the initial phenol concentration of 0.04 M and the retention time of 6 h which makes the phenol concentration in the outlet stream of the photochemical reactor not exceeding 1400 mg/L (0.0148 M). Since the bioreactor is in cascade with the photochemical reactor, the outlet stream of the later becomes the inlet stream of the former. Therefore, the biological model equations (4.24)-(4.25) were solved for the initial phenol concentration of 1400 mg/L and a retention time of 6 h for different values of α and γ, selected in their practical range.

It can be concluded from Table 4.3 that the 6 h retention time in the biological reactor does not suffice for an efficient treatment since the phenol concentration should be reduced to 3 mg/L. Table 4.3 also shows that increasing α and decreasing γ result in a more efficient treatment. The effects of α and γ will be discussed later in Sections 5.3 and 5.4.

Table 4.3: Phenol concentration (mg/L) in the outlet stream of the combined photochemical-biological system obtained by means of simulation

$\theta_C = \theta_B$ =6 h										
α	γ									
	0.005	0.01	0.03	0.05	0.07	0.10	0.12	0.13	0.14	0.15
0.25	57.20	59.93	70.74	81.16	91.02	104.46	112.48	116.21	119.76	121.47
0.30	56.84	59.21	68.65	77.89	86.78	99.21	106.82	110.41	113.86	115.53
0.35	56.58	58.69	67.15	75.50	83.63	95.20	102.42	105.86	109.20	110.82
0.45	56.23	58.00	65.12	72.23	79.25	89.49	96.04	99.21	102.32	103.84
0.55	56.01	57.56	63.81	70.10	76.38	85.65	91.67	94.62	97.52	98.95
0.65	55.86	57.26	62.90	68.61	74.34	82.88	88.49	91.26	94.00	95.35
0.75	55.75	57.03	62.23	67.51	72.82	80.81	86.09	88.70	91.30	92.59
0.85	55.66	56.86	61.72	66.66	71.65	79.19	84.20	86.70	89.18	90.42
0.95	55.60	56.73	61.31	65.99	70.72	77.89	82.69	85.08	87.47	88.66
1.0	55.57	56.67	61.14	65.70	70.32	77.34	82.04	84.39	86.73	87.90

4.3 Concluding Remarks

This chapter compared the existing biological models for phenol biodegradation. The best model recognized employed for the continuous bioreactor. Using this model for continuous bioreactor and the photochemical model developed, an overall model for the combined continuous photochemical-biological system is obtained and next chapter includes the simulation and optimization results using the overall model.

CHAPTER 5
SIMULATION AND OPTIMIZATION OF A PHOTOCHEMICAL-BIOLOGICAL PHENOL TREATMENT SYSTEM

5.1 Initial Hydrogen Peroxide Effect in CMBR

Hydrogen peroxide has a dual effect on the UV/H_2O_2 process. Figure 5.1 shows a few simulation runs carried out at a constant initial phenol concentration of 0.00043 M, using the model equations (3.14)-(3.19). Initial hydrogen peroxide concentration varied between 0 and 0.215 M in order to determine its effects on phenol removal. A wide range of H_2O_2/phenol ratio has been evaluated.

Figure 5.1 illustrates that hydrogen peroxide dramatically enhances the degradation of phenol compared to the system operating with solely UV irradiation. As in Figure 5.1, UV irradiation is responsible for about 40% of the degradation. It can be concluded from Figure 5.1 that H_2O_2 has two opposing effects on the degradation rate. It enhances the phenol degradation up to a certain point at which hydrogen peroxide becomes an inhibitor to the phenol photodegradation. At higher hydrogen peroxide concentrations, the reaction of the hydrogen peroxide with the hydroxyl radial competes with the reaction of hydroxyl radical with phenol:

$$^{\bullet}OH + H_2O_2 \xrightarrow{k_2} HO_2^{\bullet} + H_2O \tag{5.1}$$

$$^{\bullet}OH + C_6H_5OH \xrightarrow{k_{13}} \text{intremediates} \longrightarrow CO_2 + H_2O \tag{5.2}$$

H_2O_2 acts as a radical-scavenger at higher concentration than its optimum value and therefore, reduces the degradation rate. Figure 5.1 shows that, phenol degradation rate increases as the initial hydrogen peroxide concentration is raised up to R=100. However, for a H_2O_2/phenol ratio equal to 250 phenol degradation rate has already reversed its direction of variation.

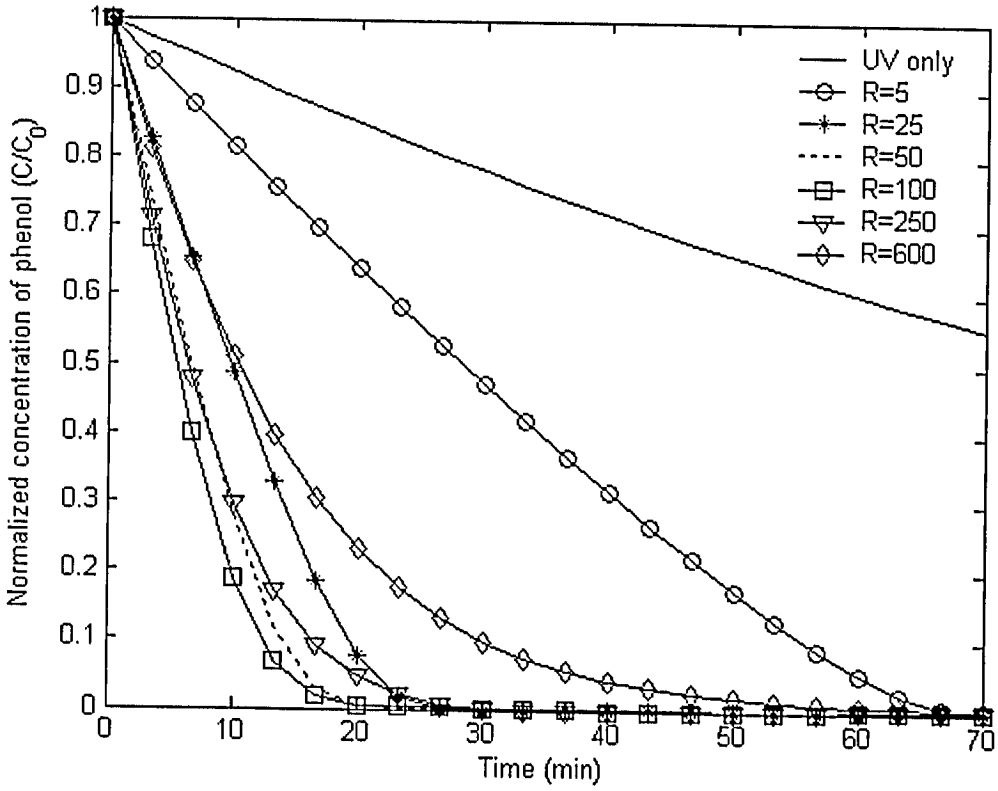

Figure 5.1: Phenol degradation at different values for R (H_2O_2 /phenol ratio), in CMBR C_0 = 0.00043 M, T=27°C.

It can be deduced from Figure 5.1 that the optimum H_2O_2 /phenol molar ratio at the selected operating conditions is between 100 and 250. The initial phenol degradation rate can be calculated from the following the equation, after substituting the concentrations with the numerical values obtained from solving the differential equations (3.14) to (3.19):

$$r_0 = \left.\frac{dX_6}{dt}\right|_{t=0} = -\left(\frac{\phi_2 I_0\left(\frac{\varepsilon_6 X_6}{\varepsilon_1 X_1 + \varepsilon_2 X_2 + \varepsilon_6 X_6}\right)}{(1-\exp(-2.303(b\varepsilon_1 X_1 + \varepsilon_2 X_2 + \varepsilon_6 X_6)))}\right) - k_{13} X_6 X_3 \qquad (5.3)$$

The following optimization function was defined in order to find the best concentration of hydrogen peroxide:

Minimize:

$$F = -\left.\frac{dX_6}{dt}\right|_{t=0} = \left(\frac{\phi_2 I_0\left(\frac{\varepsilon_6 X_6}{\varepsilon_1 X_1 + \varepsilon_2 X_2 + \varepsilon_6 X_6}\right)}{(1-\exp(-2.303(b\varepsilon_1 X_1 + \varepsilon_2 X_2 + \varepsilon_6 X_6)))}\right) + k_{13} X_6 X_3 \qquad (5.4)$$

Subject to:

$$\frac{dX_i}{dt} = r(X_i) \qquad (5.5)$$

The optimization function finds the maximum initial reaction rate subject to the photochemical model (3.14)-(3.19) while the initial conditions are shown in Table 5.1 .

Table 5.1: Initial concentrations for solving the system of differential equation in order to solve the optimization

Variables	Initial Concentration
X_1	R×0.00043 M For R=100 to 250
X_2	10^{-6}
X_3	0
X_4	0
X_5	0
X_6	0.00043 M

Plotting the initial phenol degradation rates at various H_2O_2 /phenol ratios (Figure 5.2) shows clearly that there is an optimum for phenol degradation rate.

R is the optimization variable which represents the ratio of molar concentrations of hydrogen peroxide to phenol. The exact optimum point was calculated by built-in Matlab optimization function, "fmincon". It uses a Sequential Quadratic Programming (SQP) method. The sequential quadratic programming method is dealing with nonlinear constraint optimization. In this method, the constraints would be linearized by expanding the Taylor series around the initial guess. The objective function is a quadratic approximation of the Lagrangian function, which is iteratively solved by Quadratic Programming (QP) algorithm until the convergence is achieved. The quadratic programming problem involves minimization of a quadratic function subject to linear constraints. The quadratic programming problem can be formulated as:

Minimize (with respect to x):

$$f(x) = \frac{1}{2} x^T Q x + c^T x \tag{5.6}$$

Subject to one or more equality and/or inequality constraints.

where x belongs to R^n space. Q is a symmetric, n×n matrix and c is any n×1 vector.

The difficulty of solving the quadratic programming problem mostly depends on the nature of the matrix Q. If Q is a positive semidefinite matrix, f(x) is a convex function. It means that the quadratic program has a global minimum if there is at least one vector 'x' satisfying the constraints. If the matrix Q is positive definite then this global minimum is unique. If Q is zero, then the problem becomes a linear program.

Compared to other methods for constrained optimization such as Generalized Reduced Gradient method (GRG), SQP method finds the optimum from a random starting design point. It also is capable of handling large problems involving fewer function and gradient calculations. The other advantage of SQP is that this method does not attempt to satisfy equality constraints at each iteration. As a result, it can converge faster than algorithms that consider the equality constraint at each iteration, like the GRG method.

The optimum H_2O_2 /phenol ratio for the described system calculated to be 177, which makes the best hydrogen peroxide concentration to be 0.076 M. Figure 5.3 shows phenol degradation rates at various H_2O_2/phenol ratios for different initial phenol concentrations. Optimum ratio in each case was determined in the same way as for Figure 5.2.

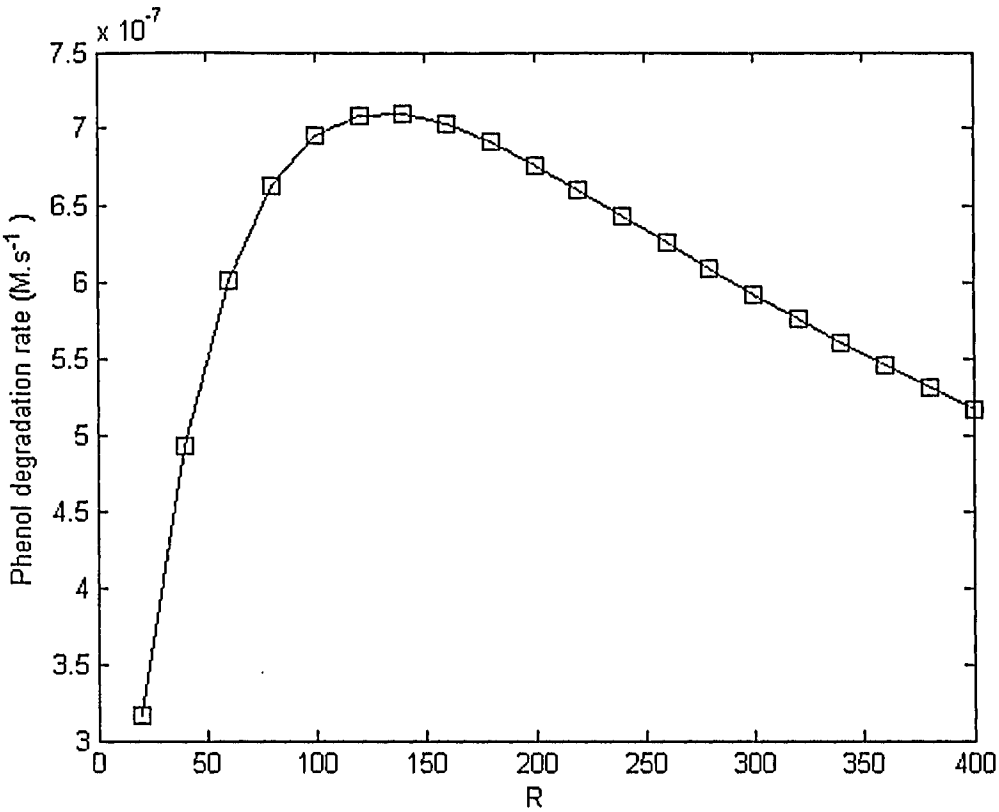

Figure 5.2: Initial phenol degradation rate versus R(H_2O_2 /phenol ratio), C_0=0.00043 M, T=27°C.

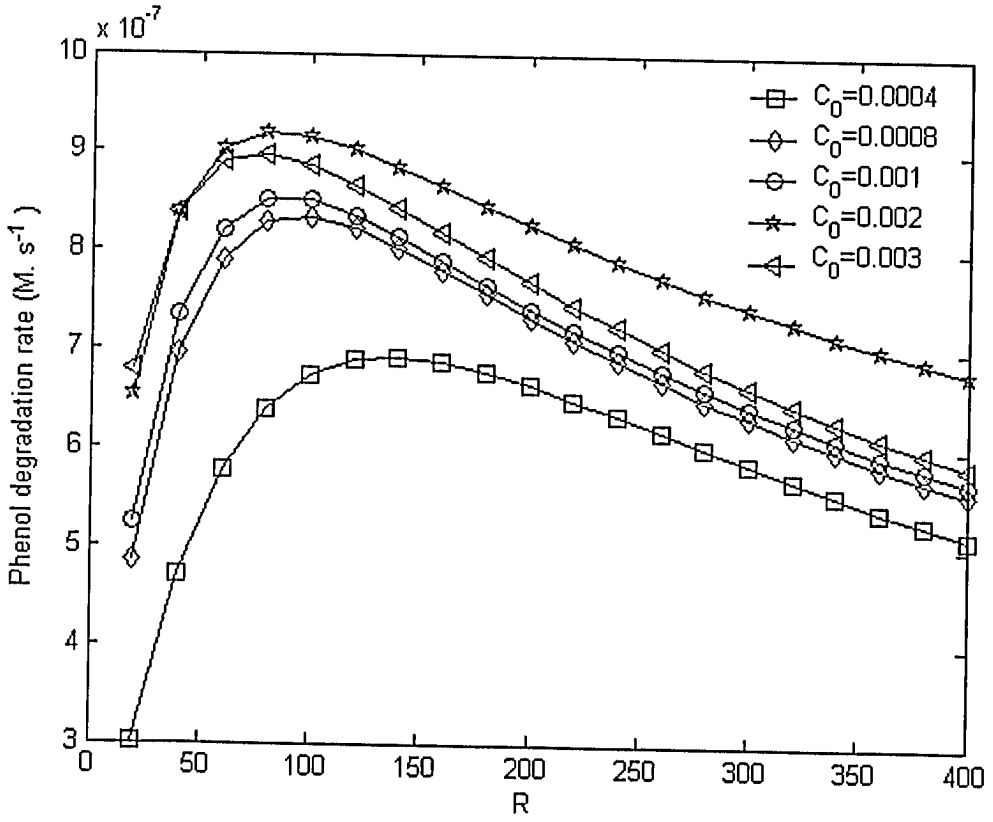

Figure 5.3: Initial phenol degradation rate versus R(H_2O_2 /phenol ratio), T=27°C.

5.2 Phenol Degradation in Continuous UV/H_2O_2 System

Residence time θ is the average time a given molecule spends in the reactor. Solving equations (3.49)-(3.54), for different values of θ allows to study the effect of θ on the efficiency of the continuous process.

Figure 5.4 shows the phenol degradation in a CSTR with a residence time between 50-2000 minutes i.e. the flow rate varies from 0.372 to 0.0093 $L.h^{-1}$. The inlet phenol and hydrogen peroxide concentrations were 0.00223 and 1.10385 M, respectively. From Figure 5.4, while it takes about 3 h for the CMBR to reduce drastically the phenol concentration, the CSTR required 30 h of retention time to reach the same level of phenol reduction.

Figure 5.5 shows the profile of phenol concentration at steady state for different residence times. It can be observed that a residence time more than about 15 h does not significantly affect phenol degradation.

5.3 Effect of Recycle on the Biological Treatment of Phenol in Activated Sludge

The recycled flow rate Q_r is set by properly adjusting the recycle ratio α. Solving the dynamic bio kinetic model presented (4.24)-(4.25), for different values of the recycle ratio α, Figure 5.6 was obtained while the biological retention time θ_B and the waste sludge ratio γ kept constant at 10 h and 0.08, respectively. Figure 5.6 shows the effect of the recycle ratio α on the process efficiency.

As the recycle ratio increases, the phenol concentration in the effluent decreases (Figure 5.6). Thus, recycling a fraction of the effluent enhances the process performance. In fact, high recycle ratio causes microorganisms to reside longer in the bioreactor and hence more time for phenol degradation to take place.

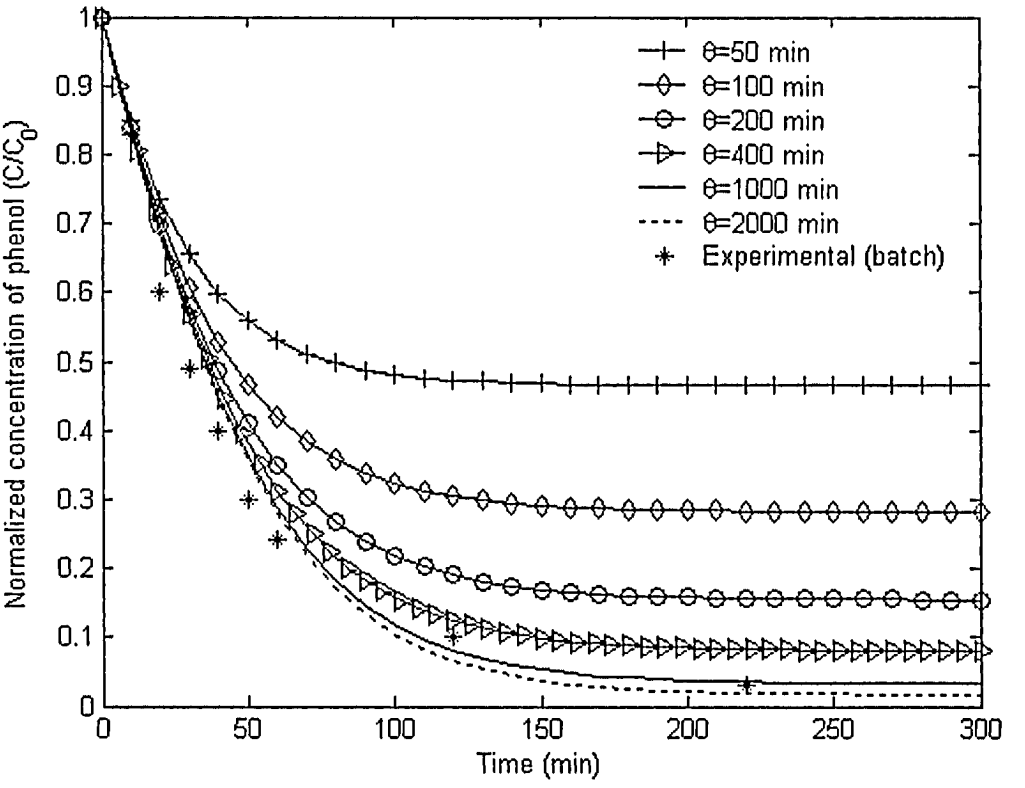

Figure 5.4: Simulated phenol degradation for different residence times in a CSTR, C_0=0.00223 M, R=495, T=27°C.

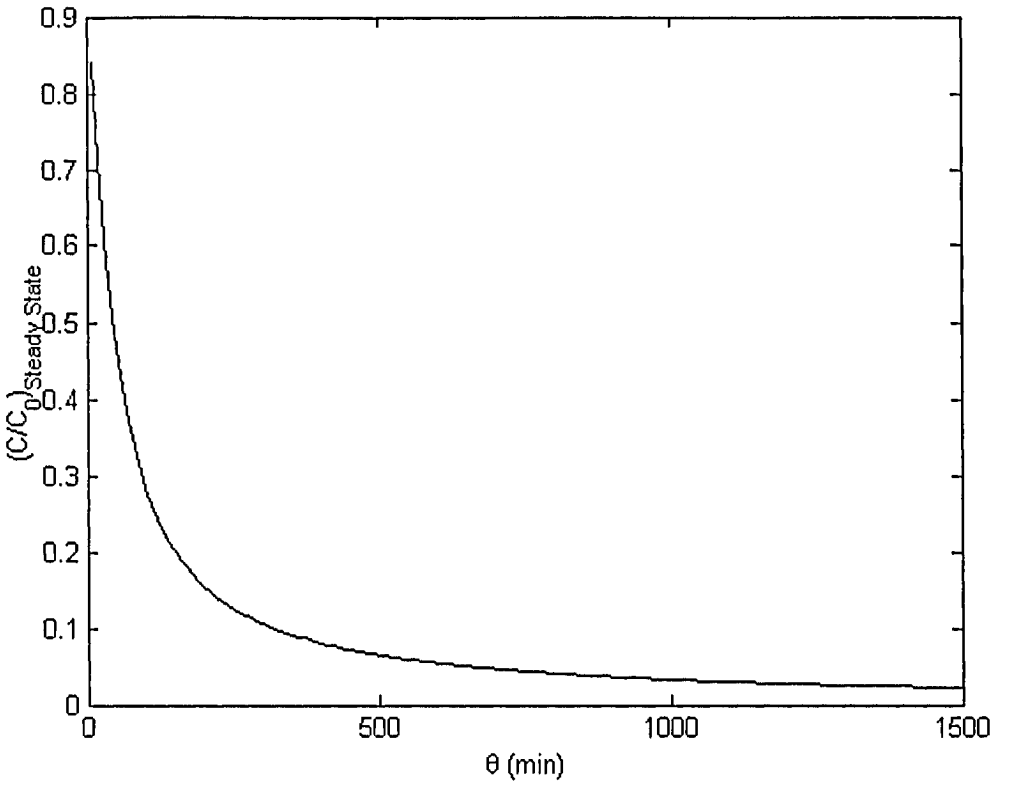

Figure 5.5: Phenol steady state concentration (simulation) in UV/ H_2O_2 CSTR, C_0=0.00223 M, R=495, T=27°C.

However, in practice, the recycle ratio should not exceed a certain limit to avoid the growth of filamentous organisms, which causes a predominant form of bulking. Bulking results in the sludge having poor settling characteristics and compactability. In practice, several techniques are used to calculate the desired return sludge flow rate. The calculations are mainly based on the sludge settling properties which should be measured at the plant. A typical range within 0.25-1 has been reported for the recycle ratio in completely mixed systems (Metcalf and Eddy, 1991).

5.4 Effect of the Sludge Wasting on the Biological Treatment of Phenol

The excess activated sludge produced each day must be wasted to maintain a given mean-cell residence time. The most common way to waste the sludge is through the return sludge line (Figure 4.2). The waste sludge flow rate is set by properly adjusting ratio of the sludge flow rate to the inlet flow rate ratio, γ. Figure 5.7 shows the effect of the waste sludge ratio γ on the process efficiency, found by the simulation. In the simulation, the set of ordinary differential equations (4.24) and (4.25) were solved by the Matlab built-in function ode45.

It can be concluded from Figure 5.7, as the waste sludge ratio increases, phenol concentration in the effluent increases linearly. Hence lowering the waste sludge flow results in more accumulation of microorganisms which increases the phenol removal. As for the recycle ratio α, in practice, limit should be imposed on the sludge waste ratio.

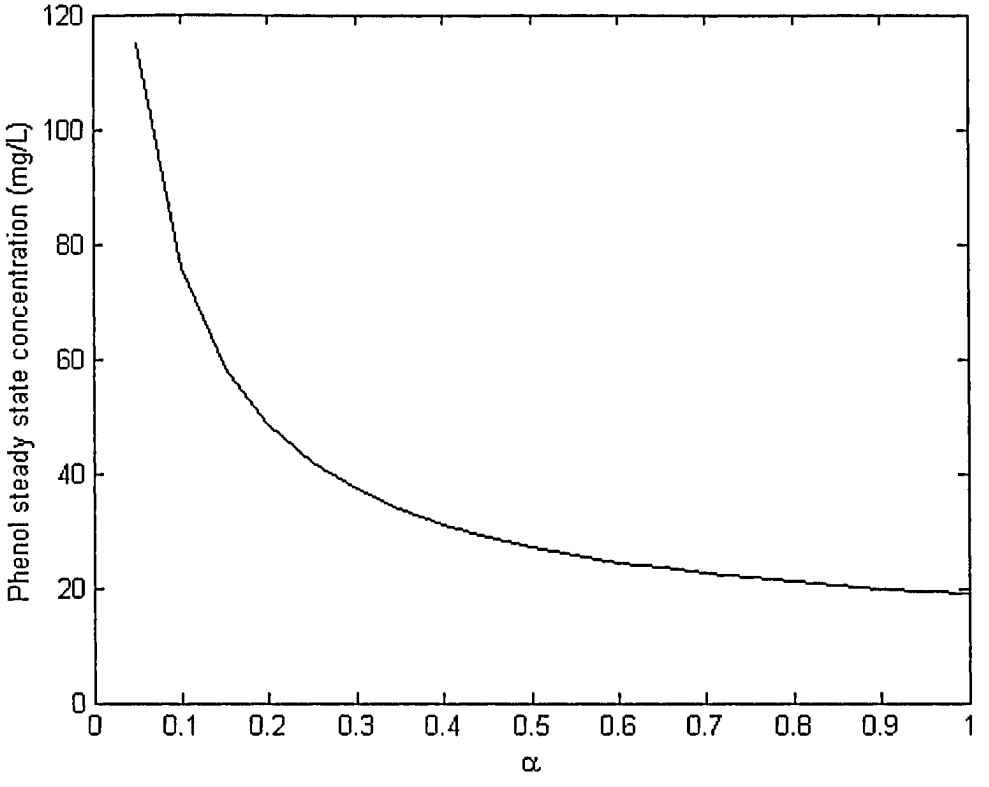

Figure 5.6: Phenol steady state concentration (simulation) versus recycle ratio α, S_0=14001 mg/L, S_0/X_0=0.8, $\gamma = 0.08$, θ_B=10 h.

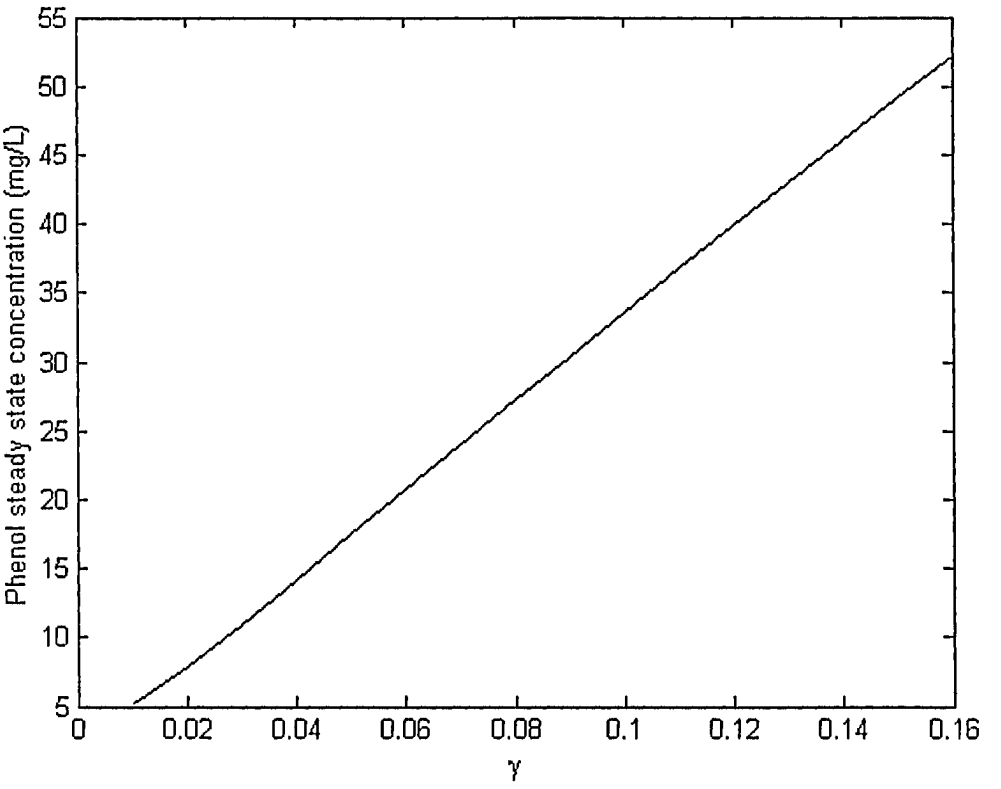

Figure 5.7: Phenol steady state concentration (simulation) versus waste sludge ratio γ, S_0=1400 mg/L, S_0/X_0=0.8, $\alpha = 0.5$, θ_B=10 h.

Assuming a low concentration of solids in the effluent, sludge retention time (SRT) can be computed using the following equation (Metcalf and Eddy, 2002):

$$SRT = \frac{VX}{Q_w X_r} \tag{5.7}$$

The sludge retention time is reported to range between 3 to 5 days in order to develop sufficient flocculent biomass for treating industrial wastewater.

Dividing the numerator and denominator both by Q_i the equation becomes:

$$SRT = \frac{\theta_B X}{\gamma X_r} \tag{5.8}$$

Using equation (4.17), the following equation can be obtained:

$$\gamma = \frac{\alpha}{\frac{SRT}{\theta_B}(1+\alpha)-1} \tag{5.9}$$

Considering the following ranges for SRT, α, and θ_B,

$$SRT : 3-5 \text{ days} \tag{5.10}$$

$$\alpha : 0.25-1 \tag{5.11}$$

$$\theta_B : \text{nearly } 12 \text{ h} \tag{5.12}$$

The ratio γ is determined to be within 0.015 to 0.15 based on the sludge allowable age range.

5.5 Optimization of Photochemical-Biological System

Complete removal of phenol through photochemical treatment incurs a high cost. As such, one may choose the more economically-appealing biological treatment process over the photochemical one. However, biological treatment alone has limited performance since phenol concentration more than a certain threshold is harmful to microorganisms. The approach adopted in this study, therefore, is to combine the photochemical and biological treatment processes so that the concentration of phenol is lowered below the required threshold through photochemical pretreatment. The photochemical-biological process considered in this study to treat wastewater using an advanced oxidation technology is a highly nonlinear and interactive system. The process has a dynamic behavior with sludge recycle in the biological unit. The recycle ratio is also important, but must be limited.

This type of problem can only be solved through an optimization scheme by solving a set of mathematical model equations. In regard with the nonlinear nature of the process with a few limitations, a nonlinear constrained optimization strategy must be opted. A constrained optimization problem is defined as:

Minimize f(x) (5.13)

Subject to:

$$g(x) = 0 \quad (5.14)$$

$$h(x) \geq 0 \quad (5.15)$$

Equation (5.13) is a scalar objective function. Equations (5.14) and (5.15) are equality and inequality constraints. The objective function or performance index defines the objective to be achieved whether it is a cost of a process or the operation time. The constraints define the model of the process and the limitations that attached to it. In this study, few objective functions were defined as follows:

a. Retention time minimization
b. Total power consumption minimization

c. Overall process cost minimization

There exist several methods to solve the optimization problem (5.13)-(5.15). Most potential gradient methods are:

- SQP (Sequential Quadratic Programming)
- GRG (Generalized Reduced Gradient)

In this study, the SQP method was used. In order to render the optimization problem numerically tractable, the "Penalty Method" was applied. The main idea of a penalty method of nonlinear programming is to convert a constrained problem into a summation of unconstrained problems as follows:

Constrained problem:

$$\begin{aligned} &\text{Minimize: } f(x) \\ &\text{Subject to: } g(x) = 0 \\ &\qquad\quad h(x) \geq 0 \end{aligned} \tag{5.16}$$

Unconstrained problem:

$$\text{Minimize } f + P(g,h,r) \tag{5.17}$$

where P(g,h,r) is a penalty function and r is a positive scalar called the penalty parameter. After the penalty function is formulated, it is minimized for a series of values of increasing r-values, thereby, forcing a sequence of minima to approach the optimum of the constrained problem. As r increases, the penalty term becomes large for any values of x that violate the equality constraints. As the penalty term grows, the values of x_i move towards the satisfying equality constrain.

5.5.1 Optimizing the Total Retention Time

For the combined photochemical-biological phenol treatment system considered in this study, different sets of retention times for reducing phenol concentration from 0.00032 to 0.04 M have been determined (Table 5.2). Since the phenol concentration entering the

bioreactor should not exceed 1400 mg/L, the smallest retention time in the photochemical reactor should be 6 hs, which is the time that photochemical reactor needs to reduce the phenol concentration from 0.04 M (3760 mg/L) to 0.015 M (1400 mg/L).

Table 5.2: Potential Retention times to reduce phenol concentration to 0.000032 M

Chemical Retention Time (h)	Phenol Concentration (M)	Phenol Concentration (mg/L)	Biological Retention Time (h)	Total Retention Time(h)
6	0.0149	1400.6	138	144
10	0.0083	780.2	110	120
14	0.00551	517.94	95	109
18	0.00409	384.46	85	103
22	0.00325	305.5	79	101
26	0.00269	252.86	74	100
30	0.0023	216.2	70	100
34	0.00201	188.94	67	101
38	0.00179	168.26	65	103
42	0.00161	151.34	63	105
46	0.00147	138.18	61	107
50	0.00135	126.9	59	109
54	0.00125	117.5	58	112
58	0.00116	109.04	57	115
62	0.00109	102.46	56	118
66	0.00102	95.88	55	121

The data presented in Table 5.2 were obtained via the algorithm presented in Figure 5.8. Figure 5.8 depicts the flowchart of the algorithm used to find the appropriate biological retention time for the efficient treatment of phenol when the retention time in the photochemical reactor is 6 h. Setting the initial phenol concentration to 0.04 M, and the photochemical retention time to 6 h, the concentration of phenol in the stream leaving the

photochemical reactor and entering the bioreactor is obtained through simulation of the photochemical model developed in equations (3.49)-(3.54). With the given initial conditions, this concentration was evaluated to be 0.0.01490 M (1400.6 mg/L). Finally, the biological retention time required to reduce the phenol concentration to 0.000032 M (3.0008 mg/L) was obtained through simulation of the biological model defined by equations (4.24) and (4.25).

Table 5.2 shows that by increasing the retention time in the photochemical reactor, the necessary treatment time in the biological reactor decreases. The minimum retention time in the photochemical reactor is about 6 h where the phenol concentration is brought to less than 3 mg/L so that it does not intoxicate the microorganisms in the subsequent units.

As in Table 5.2, the highest rate of θ_B/θ_C is about 23, therefore for a constant flow rate, the minimum volume required for the bioreactor has to be about 23 times of that the photochemical reactor, i.e. 0.3 L. In order to be on the safe side the biological reactor volume was chosen to 7.5 L in this work.

Figure 5.9 is the bar diagram showing photochemical and biological retention times, along with the total retention times. As depicted in Figure 5.9 there is an optimum for the total retention time.

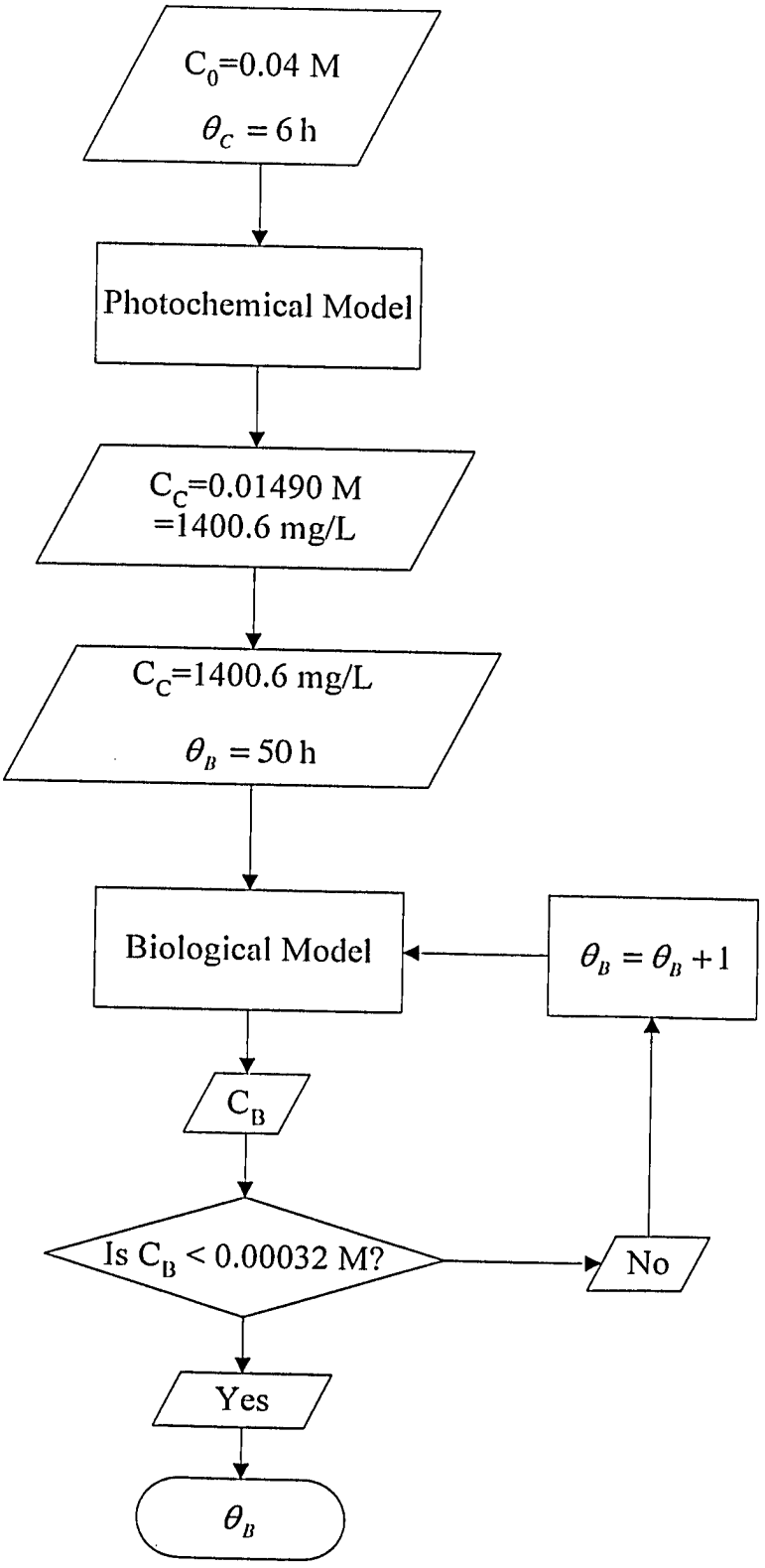

Figure 5.8. Flowchart representing the algorithm used for obtaining the appropriate photochemical and biological retention times.

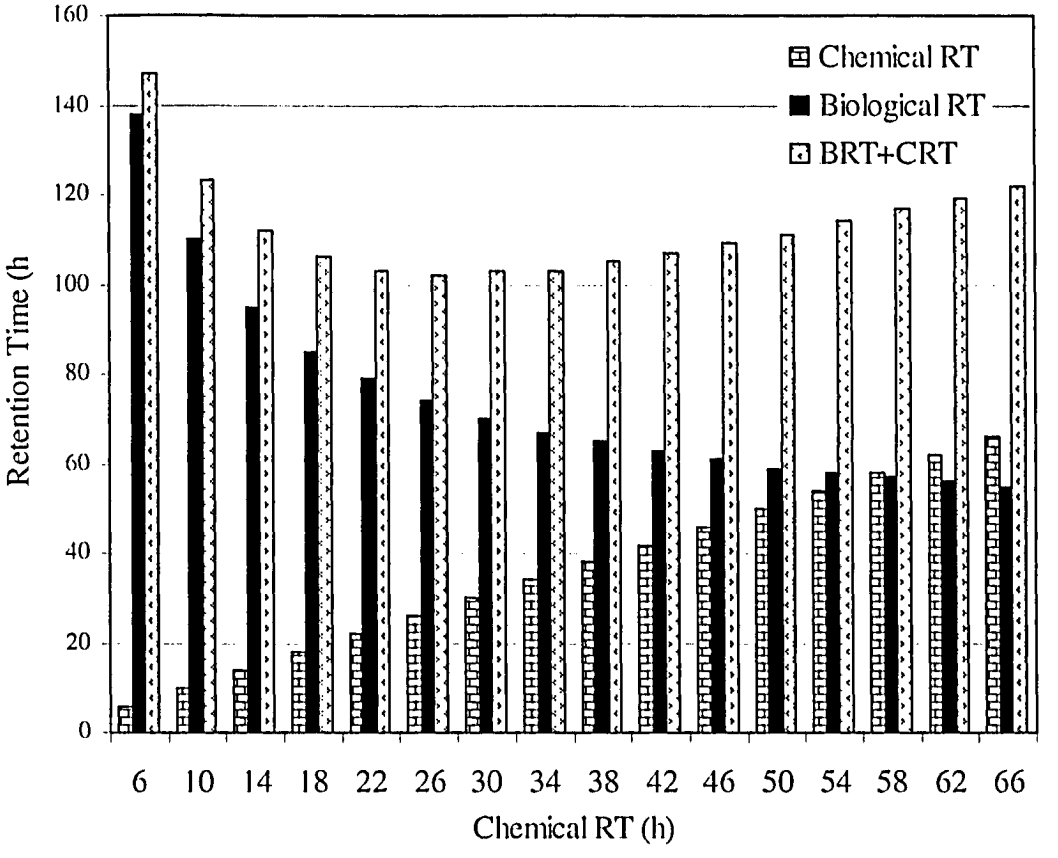

Figure 5.9: Photochemical and biological retention times resulting from different values of the photochemical retention time.

In order to determine the best option among different possibilities in Figure 5.9, an optimization scheme is defined and solved.

A. Objective function 1:

$$\text{Minimize: } F = \theta_C + \theta_B \tag{5.18}$$

Subject to:

$$\theta_C \geq 6h$$
$$\theta_B \geq 0$$
$$C_B \leq 3mg/L$$

$$\left.\frac{dZ_i}{dt}\right|_{i=1,2} = \frac{1}{\theta_B}(-Z_i) + \frac{\alpha}{\theta_B}.\frac{1-\gamma}{\alpha+\gamma}.Z_i + r(Z_i) \quad \text{Equation (4.24)} \tag{5.19}$$

$$\left.\frac{dS_i}{dt}\right|_{i=1,2} = \frac{1}{\theta_B}(S_{i0} - S_i) + r(S_i) \quad \text{Equation(4.25)}$$

$$\left.\frac{dX_i}{dt}\right|_{i=1,\ldots,6} = \theta_C(X_{i0} - X_i) + r(X_i) \quad \text{Equations (3.49)-(3.54)}$$

The optimization function is subjected to 13 constraints. First, the retention time in the photochemical reactor should be at least 6 h so that the minimum proper treatment could be done on the wastewater before entering the biological reactor. The phenol concentration in the discharged wastewater from the biological reactor should not exceed 3 mg/L based on the groundwater quality criteria (Lewis, 1993; Patrick et al., 1987). The biological retention time should be a positive number. The other 10 constraints represent the biological (4.24) and (4.25) and the photochemical (3.49)-(3.54) models.

Using the penalty method, the constraint $C_B \leq 3mg/L$ can be added to the optimization function, so that the integer part of $C_B/3$, or $\text{int}(C_B/3)$, should be zero in order to omit the penalty term $100 \times \text{int}(C_B/3)$. The optimization function F was then redefined as:

$$\text{Minimize: } F = \theta_C + \theta_B + 100 \times \text{int}\left(\frac{C_B}{3}\right) \tag{5.20}$$

Subject to:

$$\theta_C \geq 6h$$
$$\theta_B \geq 0$$

$$\left.\frac{dZ_i}{dt}\right|_{i=1,2} = \frac{1}{\theta_B}(-Z_i) + \frac{\alpha}{\theta_B}.\frac{1-\gamma}{\alpha+\gamma}.Z_i + r(Z_i) \quad \text{Equation (4.24)}$$

$$\left.\frac{dS_i}{dt}\right|_{i=1,2} = \frac{1}{\theta_B}(S_{i0} - S_i) + r(S_i) \quad \text{Equation(4.25)} \tag{5.21}$$

$$\left.\frac{dX_i}{dt}\right|_{i=1,\ldots,6} = \theta_C(X_{i0} - X_i) + r(X_i) \quad \text{Equations (3.49)-(3.54)}$$

The last term in equation (5.20) is the penalty function, which basically is the integral part of the ratio $C_B/3$. In order to find the optimum, the penalty term should be set equal to zero or equivalently the ratio $C_B/3$ should be less than unity. Therefore, at the optimum point, the constraint we meant to omit is satisfied. The penalty parameter which is chosen to be 100 in equation (5.20), is the lowest coefficient obtained to give the absolute optimum.

Applying the SQP method, the optimization problem was solved using Matlab optimization toolbox. The optimum retention times were determined to be $\theta_C = 23$ and $\theta_B = 76$, for the photochemical and biological reactors, respectively. Therefore, the overall minimum processing time is $\theta_C + \theta_B$=99 h.

5.5.2 Optimizing the Electrical Power Consumption

a) Electrical Energy per Order

No doubt, the power necessary to drive the process is important and its consumption should be kept low.Blower power requirements for aerating the bioreactor, are estimated from the air flow rate, discharge and inlet pressures, and air temperature using equation (5.22) which is based on the assumption of adiabatic conditions (Qasim, 1999):

$$P_w = \frac{wRT_1}{8.41e}\left[\left(\frac{p_2}{p_1}\right)^{0.283} - 1\right] \tag{5.22}$$

where P_w = Power requirement for the blower, kW

w = Flow rate of air, kg/s

R = Gas constants, 8.314 kJ/kmole K

8.41 = Constants for air, kg/kmole

T_1 = Absolute inlet temperature, K

p_1 = Absolute inlet pressure, atm

p_2 = Absolute outlet pressure, atm

e = Efficiency of the blower (usually 70-90 percent)

An activated sludge process needs about 1.2 kg of air per m^3 of wastewater treated (Qasim, 1999). Therefore, the required air mass flow rate is:

$$w = 1.2 \times Q \tag{5.23}$$

Typical values used for the inlet and outlet pressures are 0.95 and 1.56 atm, respectively (Qasim, 1999). Assuming an efficiency of 80%, the blower electrical power is therefore:

$$P_w = \frac{Q \times 1.2 \times 8.314 \times 303}{8.41 \times 0.9}\left[\left(\frac{1.56}{0.95}\right)^{0.283} - 1\right] = 54Q \tag{5.24}$$

In order to evaluate the efficiency in terms of the electrical energy consumed for contaminant removal, the E_{EO} is being used as the electrical energy per order for the photochemical treatment. Since the residence time is defined as follows:

$$\theta_c = \frac{V}{Q} \tag{5.25}$$

Substituting (5.25) into (2.18) gives:

$$E_{EO} = \frac{\theta_C P}{V \log(c_i / c_f)} \tag{5.26}$$

E_{EO} is the number of kW-h of electricity necessary for reducing the concentration of a contaminant in 1 m^3 by one order of magnitude. It allows an easy, and good design and scale up (Parsons, 2004).

Therefore, the electrical energy per order can also be calculated for the biological reactor, which is the energy required to decrease the pollutant concentration by one order of magnitude for a unit flow rate of wastewater emerging from the photochemical unit (1 m^3).

Since the initial concentration is fixed at 0.04 M and the discharge concentration is set to be 3 mg/L (0.000032 M), and the UV lamp power is 0.015 kW (see Table 3.5). The blower power was determined to be 54Q kW. The efficiencies E_{EO} for the biological reactor and the photochemical reactor are determined through the following equations:

$$(E_{EO})_C = \frac{\theta_C \times 0.015}{0.3 \times 10^{-3} \log(0.04/C_C)} \tag{5.27}$$

$$(E_{EO})_B = \frac{54}{\log(C_C/0.000032)} \tag{5.28}$$

Summing up (5.27) and (5.28) gives the overall process efficiency:

$$(E_{EO})_T = \frac{(E_{EO})_C \log(0.04/C_C) + (E_{EO})_B \log(C_C/0.000032)}{\log(0.04/0.000032)} \tag{5.29}$$

The terms $(E_{EO})_C \log(0.04/C_C)$ and $(E_{EO})_B \log(C_C/0.000032)$ represent each reactors contribution to the term $(\theta.P/Q)$.

b) Electrical Energy consumption

The blower and the UV lamp consume most of the electrical energy in the biological reactor and the photochemical reactor, respectively. Since the photochemical reactor has a fixed volume of 0.3 L, the electrical power required for the biological reactor may be determined as follows:

$$Q_B = Q_C = \frac{V_C}{\theta_C} = \frac{0.3\times10^{-3}}{\theta_C} \tag{5.30}$$

$$P_w = 54\times\frac{0.3\times10^{-3}}{\theta_C}(kW) \tag{5.31}$$

The electrical power for the photochemical reactor is 0.015 kW (Table 3.5). Therefore, the electrical energy consumed in the photochemical, biological, and the combined process (i.e. the summation of the consumptions in each reactor) are presented in Table 5.4.

Plotting the electrical energy consumptions versus the photochemical residence time (Figure 5.11) shows that the total electrical energy consumption has a minimum.

Table 5.3 shows the numerical values calculated for the electrical energy per order of magnitude for the photochemical, biological and the overall process. Figure 5.10 shows electrical energy consumptions required to degrade phenol one order of magnitude for the biological, photochemical and the combined process. It can be concluded from plots in Figure 5.10 that combining the photochemical process with the biological process significantly decreases the electrical energy needed for the photochemical reactor alone to degrade phenol one order of magnitude. For instance, when the residence time in the photochemical reactor is set to 10 h, the combined process degrades phenol one order of

magnitude with about 80% less electricity consumption compared to the photochemical process alone.

Table 5.3: Electrical energy per order of magnitude for the photochemical, biological and the combined process determined using the concentration C_C and the residence times.

Chemical Retention Time (h)	Phenol Concentration (M)	Biological Retention Time (h)	Electrical Energy per Order, Photochemical Reactor kWh m^{-3} per order	Electrical Energy per Order, Bioreactor kWh m^{-3} per order	Electrical Energy per Order, Combined photochemical-biological process kWh m^{-3} per order
6	0.015653	141	699.51	20.24	114.31
10	0.008959	113	732.08	22.37	178.89
14	0.006015	98	813.09	24.15	243.47
18	0.00448	88	908.78	25.63	308.05
22	0.003556	81	1009.01	26.91	372.63
26	0.002961	76	1108.92	28.06	437.21
30	0.002533	73	1209.35	29.09	501.79
34	0.002217	69	1308.84	30.03	566.37
38	0.00197	67	1408.23	30.90	630.95
42	0.00178	65	1505.12	31.73	695.53
46	0.00162	63	1603.07	32.49	760.11
50	0.00149	61	1698.69	33.23	824.69
54	0.001377	60	1793.84	33.92	889.27
58	0.001284	59	1886.05	34.63	953.85
62	0.001204	57	1981.29	35.24	1018.43
66	0.001133	56	2070.97	35.92	1083.02

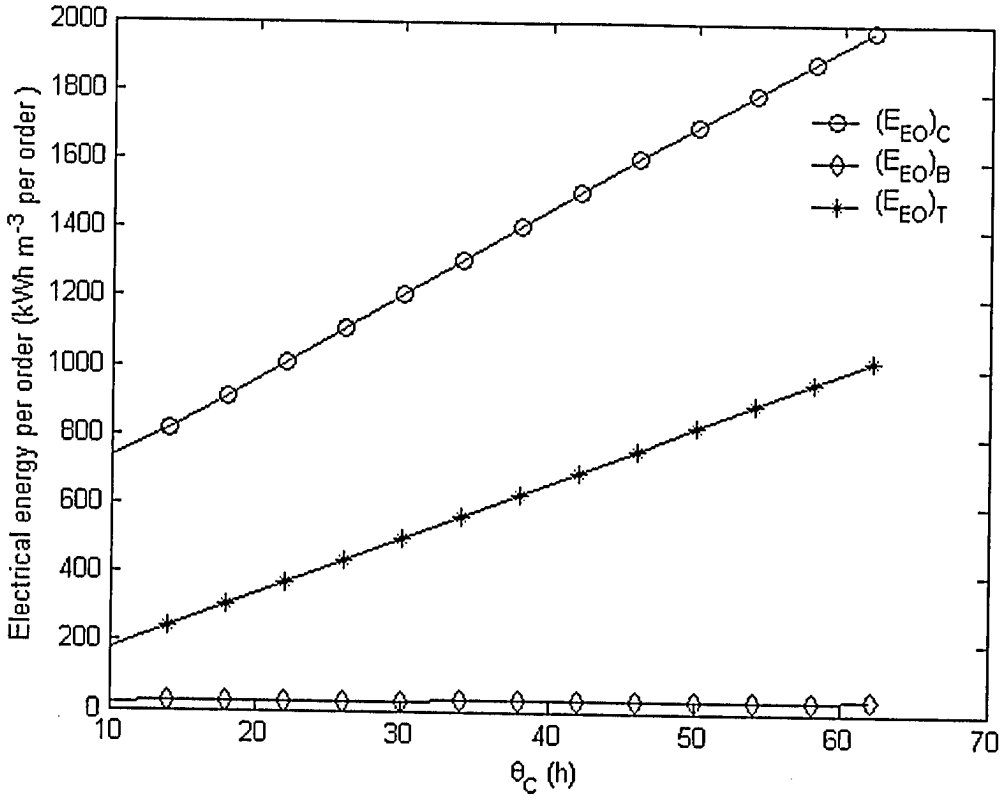

Figure 5.10: Electrical energy consumption plots for the biological, photochemical and the combined process.

Table 5.4: Electrical energy consumption in each reactor and the total energy consumption

Chemical Retention Time (h)	Phenol Concentration (M)	Biological Retention Time (h)	Electrical Energy Consumption, Photochemical Reactor (kWh)	Electrical Energy Consumption, Bioreactor (kWh)	Total Electrical Energy Consumption (kWh)
6	0.015653	141	0.090	0.373	0.463
10	0.008959	113	0.150	0.178	0.328
14	0.006015	98	0.210	0.110	0.320
18	0.00448	88	0.270	0.077	0.347
22	0.003556	81	0.330	0.058	0.388
26	0.002961	76	0.390	0.046	0.436
30	0.002533	73	0.450	0.038	0.488
34	0.002217	69	0.510	0.032	0.542
38	0.00197	67	0.570	0.028	0.598
42	0.00178	65	0.630	0.024	0.654
46	0.00162	63	0.690	0.021	0.711
50	0.00149	61	0.750	0.019	0.769
54	0.001377	60	0.810	0.017	0.827
58	0.001284	59	0.870	0.016	0.886
62	0.001204	57	0.930	0.015	0.945
66	0.001133	56	0.990	0.014	1.004

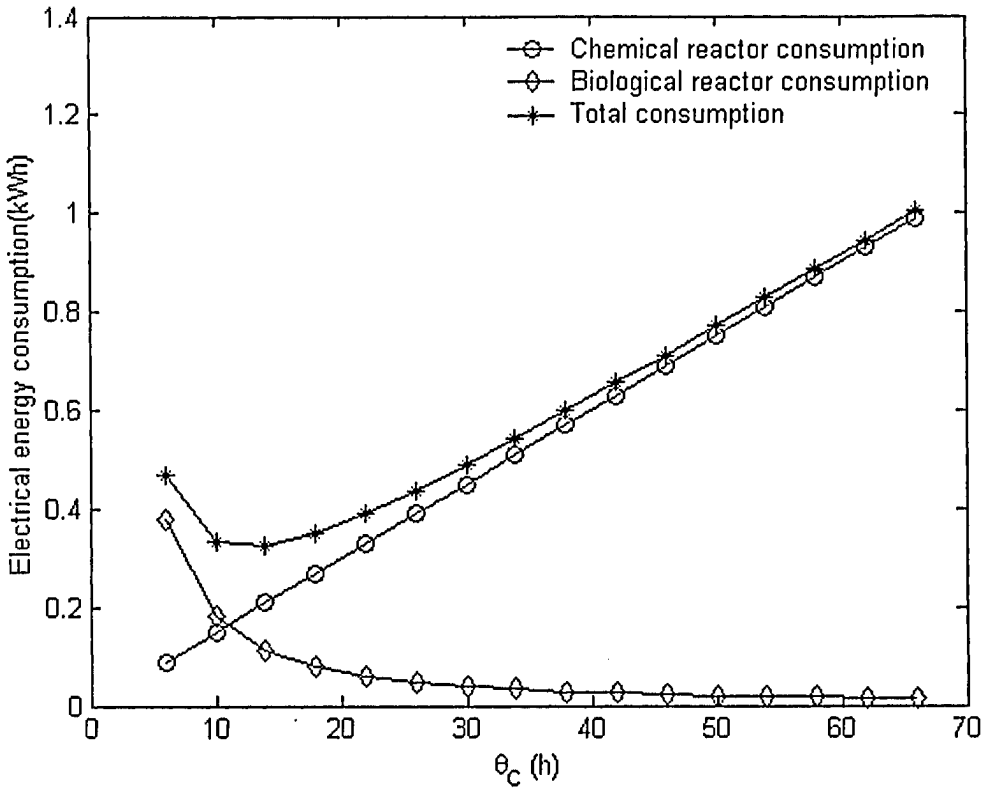

Figure 5.11: Electrical energy consumption in each reactor and total energy consumption

In order to determine the retention times giving rise to minimum energy consumption, the following optimization function was defined:

Objective function 2:

Minimize: $$E_t = E_C + E_B = 0.015\theta_c + 54\theta_B\left(\frac{0.3\times10^{-3}}{\theta_c}\right) \quad (5.32)$$

Subject to:
$$\theta_C \geq 6h$$
$$\theta_B \geq 0$$
$$C_B \leq 3mg/L$$

$$\left.\frac{dZ_i}{dt}\right|_{i=1,2} = \frac{1}{\theta_B}(-Z_i) + \frac{\alpha}{\theta_B}.\frac{1-\gamma}{\alpha+\gamma}.Z_i + r(Z_i) \quad \text{Equation (4.24)}$$

$$\left.\frac{dS_i}{dt}\right|_{i=1,2} = \frac{1}{\theta_B}(S_{i0} - S_i) + r(S_i) \quad \text{Equation(4.25)} \quad (5.33)$$

$$\left.\frac{dX_i}{dt}\right|_{i=1,\ldots,6} = \theta_C(X_{i0} - X_i) + r(X_i) \quad \text{Equations (3.49)-(3.54)}$$

where E_B and E_C are the electrical energy consumptions in the biological and the photochemical reactors, respectively, and E_t is the total electrical energy consumption. The constraints are the same as those of the optimization function (5.20). Again, penalty method is employed using the penalty parameter of 1000.

Minimize: $$F = E_t + N = 0.015\theta_c + 54\theta_B\left(\frac{0.3\times10^{-3}}{\theta_c}\right) + 1000\times\text{int}(\frac{C_B}{3}) \quad (5.34)$$

Subject to:
$$\theta_C \geq 6h$$
$$\theta_B \geq 0$$

$$\left.\frac{dZ_i}{dt}\right|_{i=1,2} = \frac{1}{\theta_B}(-Z_i) + \frac{\alpha}{\theta_B}.\frac{1-\gamma}{\alpha+\gamma}.Z_i + r(Z_i) \quad \text{Equation (4.24)} \quad (5.35)$$

$$\left.\frac{dS_i}{dt}\right|_{i=1,2} = \frac{1}{\theta_B}(S_{i0} - S_i) + r(S_i) \quad \text{Equation(4.25)}$$

$$\left.\frac{dX_i}{dt}\right|_{i=1,\ldots,6} = \theta_C(X_{i0} - X_i) + r(X_i) \qquad \text{Equations (3.49)-(3.54)}$$

where N is the penalty function which was previously explained. Using Matlab optimization tool box and solving the penalized optimization function, the optimum retention times in the photochemical and the biological reactors were determined to be $\theta_C = 15$ h and $\theta_B = 92$ h. The minimum electrical energy consumption in this case is 0.310 kWh.

5.5.3 Optimizing the Total Cost

a) Capital cost

The capital cost for a typical UV/H_2O_2 photochemical process is reported to be $85,000 plus the cost of UV lamp which is $1,500 per year (Hirvonen et al., 1998). Since the maximum allowable useful life estimate under U.S. income tax regulations is 40 years, the depreciation period is considered to be 40 years. Therefore, for 40 years of process operation, the capital cost per cubic meter is expressed as:

$$CC_C = \frac{85000 + 40 \times 1500}{40 \times (V_C/\theta_C) \times 8760} \times \left(1m^3/1000L\right) \qquad (5.36)$$

where CC_C represents the capital cost of the photochemical reactor per cubic meter for a reactor volume V_C equal to 0.0003 m^3.

Similarly, for an activated sludge plant over 40 years of operation, the capital cost per cubic meter of wastewater biologically treated is given by (Qasim, 1999):

$$CC_B = \frac{72Q + 368{,}403}{40 \times Q} = \frac{72 \times 8760\,(V_B/\theta_B) + 368{,}403}{40 \times 8760\,(V_B/\theta_B)} \times \left(1m^3/1000\,L\right) \qquad (5.37)$$

where V_B is the volume of the bioreactor which is 7.5 L.

The capital costs for the individual reactors and the total capital cost for different retention times have been determined using equations (5.36) and (5.37). The results are presented in Table 5.5.

Table 5.5: Individual and total capital costs

Chemical Retention Time (h)	Biological Retention Time (h)	Capital Cost, Photochemical Reactor ($\$ L^{-1}$)	Capital Cost, Bioreactor ($\$ L^{-1}$)	Capital Cost, Photochemical- biological Unit ($\$ L^{-1}$)
6	141	8	19	28
10	113	14	15	29
14	98	19	13	33
18	88	25	12	37
22	81	30	11	41
26	76	36	10	46
30	73	41	10	51
34	69	47	9	56
38	67	52	9	62
42	65	58	9	67
46	63	63	9	72
50	61	69	8	77
54	60	74	8	83
58	59	80	8	88
62	57	86	8	93
66	56	91	8	99

b) The Operating and maintenance cost

Considering the costs of hydrogen peroxide, utilities, labor, analytical services, and electricity, Hirvonen et al. (1998) reported the operating and maintenance costs for a typical UV/H_2O_2 system to be $2,000 per year. For 40 years of process operation, the operating and maintenance cost OMC_C per each cubic meter of wastewater which is photochemically treated is:

$$OMC_C = \frac{2000}{(V_C/\theta_C)\times 8760} \times \left(1m^3/1000L\right) \tag{5.38}$$

where V_C is the volume of the photochemical reactor (0.0003 m^3).

Similarly, the operating and maintenance cost equation at an activated sludge plant for 40 years of operation is given below (Qasim, 1999):

$$OMC_B = \frac{4.58Q + 36{,}295}{Q} = \frac{4.58\times 8760\,(V_B/\theta_B) + 36{,}295}{8760\,(V_B/\theta_B)} \times \left(1m^3/1000\,L\right) \tag{5.39}$$

where OMC_B represents the operating and maintenance costs of the biological reactor per cubic meter, and V_B is the volume of the bioreactor which is 7.5 L as it was discussed in Section 5.5.1.

The operating and maintenance cost for the individual reactors and the total operating and maintenance cost for different retention times have been determined using equations (5.38) and (5.39). The results are presented in Table 5.6.

Table 5.6: Individual and total operating and maintenance costs

Chemical Retention Time (h)	Biological Retention Time (h)	Operating and Maintenance Cost, Photochemical Reactor ($\$ L^{-1}$)	Operating and Maintenance Cost, Bioreactor ($\$ L^{-1}$)	Operating and Maintenance Cost, Photochemical- biological Unit ($\$ L^{-1}$)
6	141	5	76	81
10	113	8	61	68
14	98	11	52	63
18	88	14	47	61
22	81	17	44	60
26	76	20	41	61
30	73	23	39	62
34	69	26	37	63
38	67	29	36	65
42	65	32	35	67
46	63	35	34	69
50	61	38	33	71
54	60	41	32	73
58	59	44	31	76
62	57	47	31	78
66	56	50	30	81

c) Optimizing the total cost

Combining the objective functions (5.37)-(5.38), and (5.39)-(5.40), the overall cost for the combined process is obtained. The total costs calculated for different retention times are presented in Table 5.7.

Table 5.7: Total costs

Chemical Retention Time (h)	Biological Retention Time (h)	Total Cost, Photochemical Reactor ($\$ L^{-1}$)	Total Cost, Bioreactor ($\$ L^{-1}$)	Total Cost, Photochemical-biological Unit ($\$ L^{-1}$)
6	141	13	96	108
10	113	21	76	98
14	98	30	66	96
18	88	39	59	97
22	81	47	55	102
26	76	56	51	107
30	73	64	48	113
34	69	73	46	119
38	67	81	45	126
42	65	90	44	134
46	63	98	42	141
50	61	107	41	148
54	60	116	40	156
58	59	124	39	164
62	57	133	39	171
66	56	141	38	179

In order to determine the retention times giving the minimum total cost, penalized optimization function may be used:

Objective function 3:

Minimize:

$$F = CC_C + CC_B + OMC_C + OMC_B + N = \left(\frac{85000 + 40\times1500}{40\times(V_C/\theta_C)\times8760} + \frac{72\times8760(V_B/\theta_B)+368{,}043}{40\times(V_B/\theta_B)\times8760} + \frac{2000}{(V_C/\theta_C)\times8760} + \frac{4.58\times8760(V_B/\theta_B)+36{,}295}{(V_B/\theta_B)\times8760} \right) \left(1m^3/1000L\right) + 100\,\mathrm{int}\left(\frac{C_B}{3}\right) \quad (5.40)$$

Subject to:

$$\theta_C \geq 6h$$
$$\theta_B \geq 0$$

$$\left.\frac{dZ_i}{dt}\right|_{i=1,2} = \frac{1}{\theta_B}(-Z_i) + \frac{\alpha}{\theta_B}.\frac{1-\gamma}{\alpha+\gamma}.Z_i + r(Z_i) \quad \text{Equation (4.24)}$$

$$\left.\frac{dS_i}{dt}\right|_{i=1,2} = \frac{1}{\theta_B}(S_{i0} - S_i) + r(S_i) \quad \text{Equation(4.25)} \quad (5.41)$$

$$\left.\frac{dX_i}{dt}\right|_{i=1,\ldots,6} = \theta_C(X_{i0} - X_i) + r(X_i) \quad \text{Equations (3.49)-(3.54)}$$

Again using Matlab optimization toolbox and solving the constrained optimization problem, the optimum retention times in the photochemical and the biological reactors are found to be $\theta_C = 15.5$ h and $\theta_B = 90$ h, respectively. Figure 5.12 shows plots of the total cost versus photochemical retention time. As Figure 5.12 demonstrates, the cost of the photochemical unit is much high than the biological unit. The minimum total cost is determined to be 95 \$ L^{-1}.

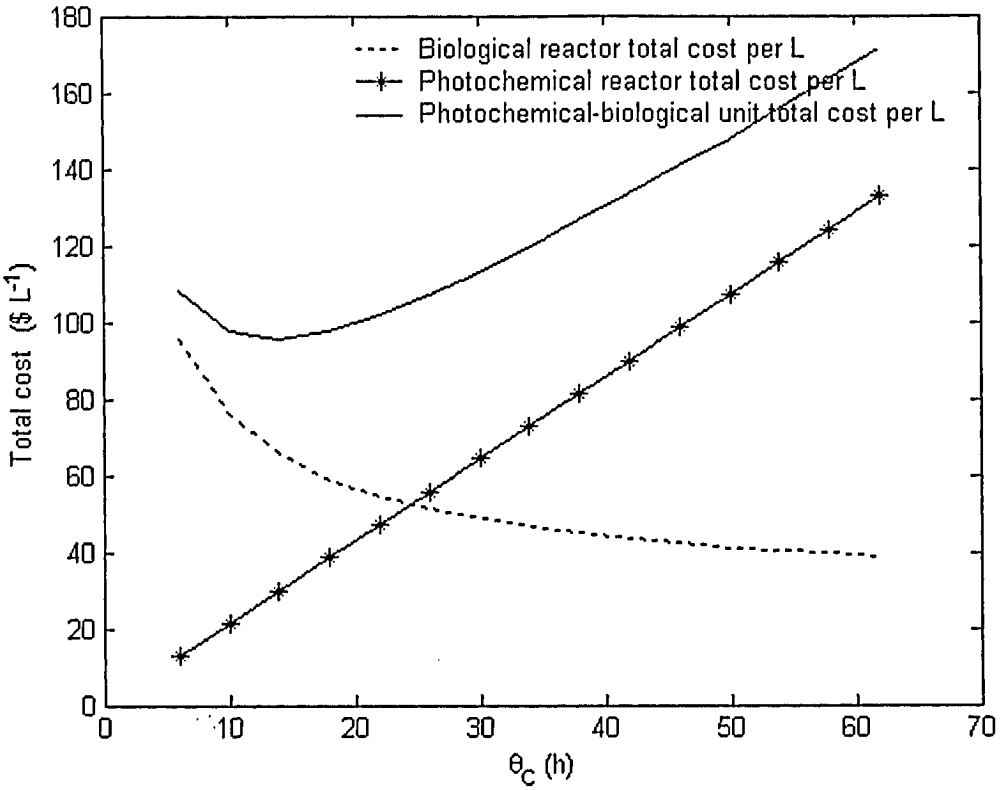

Figure 5.12: Overall cost for the combined photochemical-biological system.

CHAPTER 6
CONCLUSIONS AND RECOMMENDATIONS

6.1 Concluding Remarks

First, a dynamic kinetic model was developed for phenol degradation in an advanced oxidation system using the combination of hydrogen peroxide and ultraviolet radiation. Unlike most other kinetic models of UV/H_2O_2 oxidation process, this model did not employ the pseudo-steady state assumption. In other words, it did not assume that the net formation rate of radical species was zero. Literature data were used for photochemical parameters and photochemical rate constants. The model was validated using the experimental data from literature. The model predictions agree reasonably well with data from literature.

The model provided an understanding of the impact of the operational variables, such as hydrogen peroxide concentration on the process efficiency; consequently operational variables could be optimized using the model. An optimum hydrogen peroxide initial concentration was determined for each reactor conditions based on the organic pollutant removal efficiency of the UV/H_2O_2 process, e. g., for degradation of phenol (0.00043 M), at the light intensity of 1.516×10^{-6} $E.L^{-1}.s^{-1}$ an optimum dose of H_2O_2 was found to be 0.7611 M.

Performing parameter estimation, the kinetic rate constants for phenol degradation to catechol and hydroquinone was determined to be 9×10^{8} and 2×10^{8} $M^{-1}s^{-1}$, respectively. Also kinetic rate constants for catechol and hydroquinone degradation by hydroxyl radicals were found to be 9×10^{8} and 8×10^{7} $M^{-1}s^{-1}$, respectively.

Secondly, combining the UV/H_2O_2 process with a biological treatment allowed to achieve an efficient and cost effective degradation of phenol. With the aid of the two-step Haldane approach, biokinetic model was developed to describe the biological degradation

of phenol in an activated sludge reactor. The study demonstrated that the best design approach for an effective removal of phenol from wastewater is to cascade photochemical process with activated sludge. The combined process was simulated and the very promising results were obtained as compared to have each process generated individually.

Thirdly, the best operating conditions for the combined photochemical-biological process were determined by means of optimization. Using the SQP method, three penalized objective functions were formulated: retention time minimization, power consumption minimization, and total cost minimization. The objective functions were solved using the process limitations as the main constraints. The least total retention time possible for efficient phenol removal was determined to be 99 h and the retention times corresponding to the least electrical power consumption possible were 15 h of photochemical retention time and 92 h of biological retention time, respectively. In conclusion the overall cost function has the greatest impact on the operation of the combined process and consequently the minimum overall cost requires a residence time of 15.5 h for the photochemical reactor and a biological retention time of 90 h for the activated sludge with the recycle.

6.2 Recommendations

In the photochemical process, experiments reported in the literature so far were not intended to analyze all intermediate products and the data regarding to the known intermediates are scarce. Besides, some intermediates generated during the biological oxidation are unknown. Experimental works on the intermediate formation during phenol photochemical and biological degradation are highly recommended. More work needs to be done on kinetic and reactor modeling of both processes, photochemical and biological, with respect to the intermediate species.

Competition of chemical oxidation by the compounds and multiple substrate kinetics need to be studied further for a better understanding of the photochemical and biological processes.

In order to compare the optimization results obtained by simulation with the real optimum conditions, experimental works on the combined photochemical-biological process is also recommended.

References

1. ACGIH, "Documentation of the threshold limit values and biological exposure indices," Americal Conference of Governmental Industrial Hygienists, Cincinnati, Ohio, USA (2001).
2. R. Alnaizy and A. Akgerman, "Advanced oxidation of phenolic compounds," Advances in Environmental Research, 4 (3): 233-244 (2000).
3. Z. Alexievaa, M. Gerginova, P. Zlatevaand, and` N. Peneva, "Comparison of growth kinetics and phenol metabolizing enzymes of Trichosporon cutaneum R57 and mutants with modified degradation abilities, " Enzyme and Microbial Technology, 34: 242-247 (2004).
4. V. Arutchelvan, V. Kanakasabai, R. Elangovan, S. Nagarajan and V. Muralikrishnan, "Kinetics of high strength phenol degradation using Bacillus brevis, ", 129: 216-222 (2006).
5. J. Audureau, C. Filiol, P. Boule and J. Lemaire, "Photolyse et photo-oxidation du phenol en solution aqueuse," J. Chim. Phys. 73(6) : 513-620 (1976).
6. U. Bali, E.C. Catalkaya and F. Senguel, "Photochemical Degradation and Mineralization of Phenol: A Comparative Study," Journal of Environmental Science and Health, Part A, A38 (10): 2259-2275 (2003).
7. F. Beck, "Detection of charged intermediate of pulse radiolysis by electrical conductivity measurements," Int. J. Radiant. Phys. Chem. 1(3): 361-371 (1969).
8. H. J.Bielsky, H. J. Benon, D. E. Cabelli, L. A. Ravindra and A. B. Alberta, "Reactivity of perhydroxyl/ superoxide radicals in aqueous solution," Journal of physical and chemical reference Data, 14(4) : 1041-100 (1985).
9. J. R. Bolton, K.G. Bircher, W. Tumas and C.A. Tolman, "Figures-of-Merit for the Technical Development and Application of Advanced Oxidation Processes," Journal of Advanced Oxidation Technologies (1995).
10. L. Bolduc and W. A. Anderson, "Enhancement of the biodegradability of model wastewater containing recalcitrant or inhibitory," Biodegradation, 8(4):237-249 (1997).

11. G. V. Buxton, C. L. Greenstock, W.P. Helman and A.B. Ross," Critical review of rate constants for oxidation of hydrated electrons, hydrogen atoms and hydroxyl radicals in aqueous solutions," Journal of physical and chemical reference data, 17(2): 513-884 (1988).

12. H. S. Christensen, K. Sehested and H. Corftizan, "Reaction Hydroxyl radicals with hydrogen peroxide at ambient temperature," Journal of physical chemistry, 86: 15-88 (1982).

13. J. C. Crittenden, S. Hu, D. W. Hand and S. A. Green," A kinetic model for H_2O_2/UV process in a CMBR," Water research, 33 (10): 2315-28 (1999).

14. H. R. Devlin, and J. D. Harris, "Mechanism of the oxidation of aqueous phenol with dissolved oxygen," Industrial & Engineering Chemistry Fundamentals, 23: 387-392 (1984).

15. T. F. Edgar, Himmelblau, D. M. And L. S. Lason, ,"Optimization of chemical process,'' McGraw-Hill (2001).

16. S. Esplugas, Giménes J., Contreras S., Pascual E. and M. Rodríguez, "Comparison of different adanced oxidation technologies for phenol degradation," Water Research 36: 1034-42 (2002).

17. M. Fikar, B.Chachuat, and M. A. Latifi, "Dynamic optimization of alternating activating sludge process," Control engineering practice (2005).

18. O. Gimeno, M. Carbajo, F. J. Beltran and F.J. Rivas, "Phenol and substituted phenols AOPs remediation," Journal of Hażardous materials, B119: 99-108 (2005).

19. P. R. Gogate and A. B. Pandit, "A review of imperative technologies for wastewater treatment 1: oxidation technologies at ambient conditions," Advances in Environmental Research 8 : 501-551 (2004).

20. O. J. Hao, M. H. Kim, E. A. Seagren and H. Kim, "Kinetics of phenol and chlorophenol utilization by *Acinetobacter* species," Chemosphere, 46 (6): 797-807 (2002).

21. A. Hirvonene, T. Tuhkanen, M. Ettala and P. Kalliokoski, "Evaluation of a field scale UV/H_2O_2 oxidation system for purification of groundwater contaminated with PCE," Environmental Technology 19:821-828 (1998).

22. T. F.L. Ho, J. R. Bolton and E. Lipczynska-Kochany, "Quantum yields for the photodegradation of pollutants in dilute aqueous solution: phenol, 4-chlorophenol and N-nitrosodimethylamine," Journal of advanced oxidation technology, 1(2):170-178 (1996).

23. R. B. Jordan, "Reaction mechanisms of inorganic and organometallic systems," Oxford University Press (1998).

24. W. H. Koppenol, J. Butler and J. W. L. Van Leeuwen, "The Harber-Weiss Cycle," Journal of Photochemistry and Photobiology, 28: 655-660 (1978).

25. A. Kumar, S. Kumar and S. Kumar, "Biodegradation kinetics of phenol and catechol using Pseudomonas putida MTCC 1194," Biochemical Engineering Journal, 22:151-159 (2005).

26. J. Laat, and H. Gallard, "Catalytic decomposition of hydrogen peroxide by Fe(III) in homogeneous aqueous solution: mechanism and kinetic modeling," Environmental Science and Technology,33(16) :2726-2732 (1999).

27. Lewis publishers, "48th Purdue industrial waste conference proceedings," Chelsea, Michigan 48118, printed in USA (1993).

28. A. Nuhoglu, and B. Yalchin, "Modelling of phenol removal in a batch reactor," Process biochemistry, 40: 1233-1239 (2005).

29. O. B. Oroirien, B. Amigun, T. V. Ojumu, O. A. Ogunkunle, O.A. Adetunji, E. Betiku and B. O. Solomon, "Substrate inhibition kinetics of phenol degradation by Pseudomonas aeruginosa and Pseudomonas fluorescence , " Biotechnology, 4 (1): 56-61 (2005).

30. T. Oppenlander, " Photochemical purification of water and air," Wiley (2003)

31. R. H. Perry, D. W. Green and J. D. Maloney, "Chemical Engieer's Handbook," McGraw-Hill, New York (1981).

32. S. Parsons, "Advanced Oxidation Processes for Water and Wastewater Treatment", IWA publishing (2004).

33. R. Patrick, E. Ford and J. Quarles, "Groundwater Contamination in the United States," University of Pennsylvania Press, (1987).

34. S. R. Quasim, "Wastewater treatment plants," Technomic publishing co., (1999).

35. K. F. Reardon, D.C. Mosteller and J. D. B. Rogers," Biodegradation kinetics of benzene, Toluene, and phenol as single and mixed substrates for Pseudomonasputida F1," Biotechnology and Bioengineering 69(4):385-400 (2000).

36. S. Rigopoulos, and P. Linke, "Systematic development of optimal activated sludge process design," Computer and chemical engineering, 26: 585-597 (2002).

37. C. K. Scheck, and F. H. Frimmel, "Degradation of phenol and salicylic acid by ultraviolet radiation / hydrogen peroxide," Water Research, 29(10): 2346-2352 (1995).

38. K. Schested, O.L. Rasmussen and H. Fricke, "Rate constants of OH with HO_2, O^-_2 and $H_2O^+_2$ from hydrogen peroxide formation in pulse-iradiated oxygenated water," Journal of physical chemistry, 72: 626-631 (1968).

39. J. P. Scott, and D. F. Ollis, "Engineering models of combined chemical and biological processes," Journal of Environmental Engineering, 122(12): 1110-14 (1996).

40. S. Seker, H. Beyenal, B. Salih and A. Tanyolac, "Multi substrate growth kinetics of Pseudomonas putida for phenol removal," Applied Microbiology and Biotechnology, 47: 610-614 (1997).

41. R. Stegmann, G. Brunner, W. Calmano, G. Matz, "Treatment of contaminated soil," Springer, Germany, (2004).

42. A. Sugiarto, and T. Ohshima, "Advanced oxidation processes using pulsed streamer corona discharge in water," Thin solid films, 407(1):174-178, (2002)

43. G. B. Tabrizi, and M. Mehrvar, "Integration of advanced oxidation technologies and biological processes: recent developments, trends, and advances," Journal of Environmental Science and Health, Part A 39(11-12): 3029-3081 (2004).

44. G. Tuncel, and C. Nergiz, "Antimicrobial effect of some olive phenols in a laboratory medium," Letters in Applied Microbiology, 17(6): 300-302 (1993).

45. G. Vazquez-Rodriques, C. B. Youssef and J. Waiss,am-Vilanova, " Two-step modeling of the biodegradation of phenol by an acclimated activated sludge," Chemical Engineering Journal, 117: 245-252 (2006) .

46. P. Venkataraman, "Applied optimization with MATLAB programming," Wiley, (2002).

47. S. J. Wang, and K.C. Loh, " Modeling the role of metabolic intermediates in kinetics of phenol biodegradation" Enzyme and Microbial Technology 25: 177-184, (1999).

48. J. Weinstein, H. J. Benon and H. J. Bielsky, "Kinetics of the interaction of HO_2 and O^-_2 radicals with hydrogen peroxide. The Harber-Weiss reaction," Journal of the American Chemical Society 101:58-62 (1979).